UPPSALA
UNIVERSITET

UPTEC W 18 015
Examensarbete 30 hp
April 2018

Hydrometeorological extremes in the Adige river basin, Italy

David Gozzi

ABSTRACT

Hydrometeorological extremes in the Adige river basin, Italy

David Gozzi

This study aimed at describing the characteristics of daily precipitation and discharge extremes in the Adige river basin at the city of Trento. Annual maximum series for the period 1975−2014 were analyzed in terms of trends, seasonality indices and L-moments. A Mann-Kendall trend analysis showed a weak but significant signal of decreasing extremes; the percentages of sites with significant negative trends were overall larger than the significance levels. Precipitation extremes were characterized primarily by autumn storms, while floods had a stronger seasonality with peaks occurring predominantly in June and July which indicated that the timing not solely explained by rainfall maxima. The Adige basin was found to be a homogenous region with respect to precipitation, but the results did not support a corresponding assumption for discharge. A regional frequency analysis was performed for precipitation data and found both the Pearson type III and generalized normal distributions to be adequate regional frequency distributions. The extreme daily precipitation at Trento with a 100-year return period was estimated to be between 114 and 148 mm/d.

Keywords: Hydrometeorological extremes, precipitation, discharge, floods, seasonality, L-moments, regional frequency analysis, trend analysis, Adige river.

Department of Earth Sciences, Program of Air, Water and Landscape Sciences, Uppsala University, Villavägen 16, SE-752 36, Uppsala, Sweden.

REFERAT

Hydrometeorologiska extremvärden i Adigeflodens avrinningsområde, Italien
David Gozzi

Egenskaperna hos extremvärden av dygnsnederbörd och -vattenföring i Adigeflodens avrinningsområde vid staden Trento undersöktes. Serier med årsmaxima för perioden 1975–2014 analyserades med avseende på trender, säsongsindex och L-moment. Trendanalys med Mann-Kendallmetod antydde en svag men signifikant signal om minskande extremvärden, då andelen mätstationer med signifikant negativa trender överlag var större än signifikansnivån. Den extrema nederbörden karakteriserades huvudsakligen av höststormar, medan vattenföringen hade en starkare säsongsbundenhet då maxima inträffade främst under juni och juli. Vattenföringens extremvärden kunde därmed inte enbart förklaras av nederbördsmaxima. Avrinningsområdet kunde betraktas som en homogen region för nederbörd, men resultaten gav inte stöd åt ett motsvarande antagande för vattenföring. En regional frekvensanalys genomfördes för nederbördsdata och visade att Pearson typ III och den generaliserade normalfördelningen var lämpliga regionala sannolikhetsfördelningar. Över Trento uppskattades den extrema dygnsnederbörden med en återkomstperiod på 100 år till mellan 114 och 148 mm/d.

Nyckelord: Hydrometeorologiska extremvärden, nederbörd, vattenföring, säsongsindex, L-moment, regional frekvensanalys, trendanalys, Adigefloden.

Institutionen för geovetenskaper, luft-, vatten och landskapslära, Uppsala Universitet, Villavägen 16, 752 36, Uppsala, Sverige.

PREFACE

Korbinian Breinl has been the supervisor for this thesis and Giuliano Di Baldassarre the academic supervisor, both at the Department of Earth Sciences at Uppsala University. The author wishes to thank them for their guidance over the course of the project, and also to acknowledge the University of Trento who provided the data used in the study.

UPTEC W 18 015, ISSN 1401-5765
Published digitally at the Department of Earth Sciences, Uppsala University, Uppsala 2018

POPULÄRVETENSKAPLIG SAMMANFATTNING

Alperna är ett område som ofta är utsatt för extremväder och som upplevt flera svåra översvämningar de senaste åren till följd av häftiga regn. Flera av Europas större floder har sina källor här vilket gör att effekterna också drabbar områden nedströms. I november 2014 orsakade en kraftig storm dödsfall och stora skador i Schweiz och i norra Italien. Efter regnoväder i augusti 2005 brast fördämningar till flera floder i Sydtyskland och många tvingades fly eller evakueras. Samtidigt omkom flera människor i Österrike och Schweiz efter att regnen utlöst jordskred.

I Italien räknas ovädret 1966 som en av de allvarligaste väderkatastroferna under 1900-talet. Stormen orsakade stora skador och många dödsfall i de centrala och nordöstra delarna av landet. Bland annat översvämmades staden Trento i Alperna som ligger längs Italiens näst längsta flod, Adige. För att motverka Adigeflodens skadeverkningar har man byggt vallar längs flodens sträckning genom Lagarinadalen och flera dammar i området kan dämpa höga flöden. Här finns även många hydrologiska och meteorologiska stationer som mäter vattenföring, nederbörd, temperatur och andra variabler.

För att förebygga framtida översvämningar och dimensionera infrastruktur och byggnadsverk är det viktigt att förstå sannolikheten att en händelse av en viss magnitud ska inträffa. En sådan uppskattning kräver att man känner till sannolikhetsfördelningen, det vill säga den matematiska beskrivningen av hur sannolika observationer av olika magnituder är. Analyser av statistik för uppmätta hydrometeorologiska variabler är ett vanligt sätt att ta reda på en sådan sannolikhetsfördelning, och därför en viktig del i bedömningar av översvämningsrisk.

I det här arbetet undersöktes extremvärden av nederbörd och vattenföring i avrinningsområdet till Adigefloden ner till staden Trento. Analyserna har utförts på dataserier med årsmaxima, det vill säga de maximala dygnsvärdena som observerats varje år under perioden. Metoderna bakom resultaten kan i korthet beskrivas enligt följande. (1) Sannolikhetsfördelningen för nederbörd togs fram genom en regional frekvensanalys. Ett vanligt problem med miljödata är att observerade serier av årsmaxima är korta. Regional frekvensanalys bygger på att serier från olika stationer kan slås ihop och bedömas tillsammans om de är tillräckligt lika, vilket gör en sådan metod lämplig för korta serier. De matematiska parametrarna till fördelningen uppskattades med så kallade L-moment, som jämfört med andra metoder visats prestera väl då datamängden är liten. (2) En trendanalys genomfördes för att undersöka om årsmaxima har ökat eller minskat under den observerade perioden. Mann-Kendalls metod användes då denna inte kräver att serien är normalfördelad, vilket sällan är fallet för miljödata. (3) Säsongsvariationen av årsmaxima för nederbörd och vattenföring beskrevs med säsongsindex. De är mått på vilket tid på året som maxima inträffar i medeltal, samt hur mycket datumet varierar.

Tre huvudsakliga resultat kan lyftas fram. (1) Sannolikhetsfördelning för nederbörd visade på att den maximala dygnsnederbörden som kan väntas falla över Trento sett över en 100-årsperiod är mellan 114 och 148 mm/d. Detta kan användas i vidare studier som indata till modeller som kan beräkna flodens extremflöden, eller för bedömningar av klimatförändringars effekter på vattenresurser i regionen. Resultaten indikerar även (2) att magnituden av extremvärdena minskat under den undersökta perioden 1975–2014, samt (3) att det utöver extremnederbörd sannolikt är snösmältning som styr vilken tid på året som de högsta flödena inträffar.

TABLE OF CONTENTS

1. INTRODUCTION

The Adige river in the north-eastern Italian Alps had its latest severe flood in 1966 following a cyclonic storm considered to be the most important hydrometeorological event in Italy in the last century (Malguzzi et al., 2006). The synoptic scale storm caused damages and casualties over the whole of central and northeastern Italy, including the flooding of the town of Trento on the Adige river.

Extreme precipitation and discharge events such as this pose considerable risks to human life, economy and infrastructure. In the Alpine region, large floods have been shown to be more frequent than in the past and may become even more frequent under global warming (Allamano, 2009). Although, predictions are particularly difficult to make here since data are sparse and the spatial variability of the hydrological environment is significant (Parajka, 2005). Even so, the spatial and temporal patterns of the extremes need to be characterized for flood risk analyses, assessments of climate change effects and water resource management.

An important characteristic of hydrometeorological extremes is the seasonality, i.e. the tendency for events to occur in certain parts of the year. Seasonality has an impact on both the precipitation inputs to a catchment and its soil wetness and therefore has a great influence on the magnitude and timing of annual maximum discharge peaks (Blöschl et al., 2013). The seasonality of hydrological processes has been the focus of recent studies on both the European scale (Blöschl et al., 2017; Parajka et al., 2010) and the scale of Alpine catchments (Turkington et al., 2016).

A common way to characterize extremes is by estimating the frequency of events. Knowledge of the magnitude and probable frequency of recurrence is needed for planning decisions. Especially for engineering purposes, frequency analysis of extreme hydrometeorological events is needed for proper design of structures such as dams, levees, waterworks and sewage disposal plants (Dalrymple, 1960).

The statistical approach to frequency analysis of floods has been under debate since its introduction (see Klemeš (2000) and references therein), where a major criticism concerns the extrapolation beyond the range of observations for higher return periods. The issue of short records can be mitigated by so called regional frequency analysis. Related samples of data can be analyzed together, as a region, if the event frequencies are similar (Hosking and Wallis, 1997). Thus, the large sampling errors associated with short records can be reduced.

The use of L-moment statistics is a common approach in regionalization studies (e.g. Adamkowski, 2000; Hailegeorgis et al., 2013). Conventional moments such as mean, variance, skewness and kurtosis describe the scale and shape of a probability distribution; L-moments are analogues to these but have been shown to characterize a wider range of

distributions and having a better performance for small samples (Hosking and Wallis, 1997).

Central to regionalization is the concept of homogeneity, i.e. sufficiently similar frequency distributions among the pooled samples. Regional analysis studies of extreme precipitation have found significant relationships between L-moments and mean annual precipitation, and successfully used this to group sites into homogenous regions (e.g. Schaefer, 1990; Di Baldassarre et al., 2006).

The Italian VA.PI. project identified a nationwide approach for frequency analysis of extreme rainfall and floods based on data records up to the 1980s (COST, 2012). The resulting reference procedure for regional flood frequency estimation adopts the use of hierarchical regions. Italy is delineated into regions of the first level, where shape parameters are considered constant, and sub-areas of the second level where dispersion (e.g. variance) is assumed constant. The Adige basin belongs to the Triveneto region which is considered homogenous at both the first and second level. Manfreda and Fiorentino (2008) applied the VA.PI. procedure to the Adige river and assumed the flood data to be homogenous, while a recent study of Triveneto finds this larger region to be heterogeneous (Persiano et al., 2016). It is therefore interesting to revisit the homogeneity assumption for the Adige basin.

1.1. PURPOSE AND RESEARCH QUESTIONS

This study aimed at describing the characteristics of daily precipitation and discharge extremes in the Adige river basin down to the city of Trento. Annual maximum (AMAX) series for the recent 40-year period 1975-2014 were developed and analyzed in terms of temporal trends, their distributional properties and the seasonality of the events.

The research questions were as follows.

1. Do the AMAX series exhibit any trends?
2. (a) Can the catchment be considered a homogenous region with respect to precipitation and discharge? (b) If so, which frequency distribution is in accordance with the data? (c) And what are the expected precipitation depths or discharge peaks for return periods up to 100 years?
3. (a) What does the sample L-moments say about the spatial distribution of the extremes in the catchment? (b) Is there a relationship between L-moments of precipitation extremes and the mean annual precipitation?
4. (a) What is the seasonality of annual maxima and how strong is it? (b) What does the seasonality say about precipitation as a driving process of floods in the basin? (c) Have there been any shifts in the seasonal timing of extremes?

1.2. LIMITATIONS

- Only daily data have been analyzed. Available sub-daily series were found to be too short.

- Results can only describe flood characteristics in terms of precipitation, and not with regard to other flood generation process such as soil moisture and snow melt.
- Minimum required length of record (20 years) was kept short due to scarcity of discharge data.

2. THEORY

2.1. BLOCK MAXIMA

The block maxima (BM) method is one of two fundamental approaches in extreme value theory, the other being peak-over-threshold (Ferreira and Haan, 2015). The BM method consists of dividing the observation period into equally sized and non-overlapping periods and restricting the analysis to the maximum observations in each period – e.g. annual maxima. Ferreira and Haan (2015) compared the two methods applied with L-moments (see section 2.8) and suggested that the BM method is generally more efficient under many practical conditions.

2.2. FLOOD GENERATION PROCESSES

Extreme rainfall processes are a form of climate forcing on flood generation (Blöschl et al., 2013). Events may be produced by smaller scale convective storms, covering a few kilometers and lasting a few hours or less with high intensities. They can also be produced by atmospheric mechanisms on larger scales caused by dynamic uplifting or, in mountainous regions, by orographic effects. These storms cover larger spatial scales, have a longer duration and lower intensities. In colder regions, snowmelt and rain on snow events are important generation processes as well (Merz and Blöschl, 2003).

The storm durations relative to the mean response time of a catchment is a key influence on flood peaks. The largest floods typically occur when the storm duration is equal to or greater than the response time of the catchment, since this may give rise to a resonance effect (Blöschl et al., 2013).

2.3. TREND ANALYSIS

The Mann-Kendall (MK) test is a nonparametric test for monotonic trends. Mann (1945) used the significance test of Kendall's correlation coefficient τ with time as the independent variable. The test statistic S is computed for all possible data pairs and measures the monotonic dependence of the dependent variable y on time. It compares the number of pairs where y increases with time, and the number of pairs when y decreases with time. The null hypothesis of no change is rejected if S, and therefore Kendall's τ of y versus time, is found to be significantly different from zero (Helsel and Hirsh, 2012).

The MK trend test is often suitable for environmental data since it is robust to outliers and missing values, and no assumption of normality is required (Helsel and Hirsh, 2012). However, there must be no serial correlation for the p-values of the trend significance test to be correct. A positive serial correlation increases the likelihood of detecting a significant trend when none may exist, i.e. a type I error in the significance test (Yue et al.,

2002). The reverse is true for negative serial correlation, which may cause underestimation of significant trends (type II error). Moreover, the presence of trends affects the detection of serial correlation. Yue et al. (2002) suggests a modified MK test for serially correlated data which includes detrending the series prior to pre-whitening (i.e. removal of serial dependence), to accurately estimate the serial correlation.

The rate of change of a trend can be assessed by the nonparametric slope estimator of Theil (1950) and Sen (1968). The null hypothesis is stated as a significant test for the slope coefficient β, in similar manner as for Kendall's τ. Blöschl et al. (2017) use an adjusted β estimator for trend estimation of timing of annual maximum events, which accounts for the circular nature of dates. The slope estimator is calculated as the median of the differences between dates D over all possible pairs i and j in the AMAX series,

$$\beta = median\left(\frac{D_j - D_i + k}{j - i}\right) \text{ with } k = \begin{matrix} -\bar{m}\ if\ D_j - D_i > \bar{m}/2 \\ \bar{m}\ if\ D_j - D_i < \bar{m}/2 \\ 0\ otherwise \end{matrix}, \quad (1)$$

where k adjusts for circularity and $\bar{m}$ is the average number of days per year (to account for leap years). D is given in day numbers (January 1 corresponding to D=1 and December 31 to D=365 or D=366). Unit of β is days per year.

2.4. SEASONALITY ANALYSIS

The seasonality analysis of annual maximum precipitation and discharge is based on directional statistics (Mardia, 1972) which can account for the fact that the first and last days of the year have adjacent values in the time series. Bayliss and Jones (1993) adapted the directional statistics for analysis of extreme hydrological events and introduced indices that reflect the mean date of occurrence of the events and its variability. Hall and Blöschl (2017) use the following procedure to estimate these indices.

The date of occurrence D_i of an event in year i is expressed as an angular value θ_i by plotting it on a unit circle in polar coordinates:

$$\theta_i = D_i \frac{2\pi}{m_i} \text{ where } 0 \le \theta_i \le 2\pi, \quad (2)$$

where D_i=1 corresponds to January 1 and $D_i = m_i$ to December 31, and m_i is the number of days in year i. The mean x- and y-components of the sample of events are obtained by

$$\bar{x} = \frac{1}{n}\sum_{i=1}^{n} \cos(\theta_i) \quad (3)$$

$$\bar{y} = \frac{1}{n}\sum_{i=1}^{n} \sin(\theta_i) \quad (4)$$

where n is the total number of events at a station. The mean date of occurrence D_{mean} at a station is defined as

$$D_{mean} = \begin{cases} \tan^{-1}\left(\frac{\bar{y}}{\bar{x}}\right) \cdot \frac{\bar{m}}{2\pi} & if \quad \bar{x} > 0, \ \bar{y} \geq 0 \\ \left(\tan^{-1}\left(\frac{\bar{y}}{\bar{x}}\right) + \pi\right) \cdot \frac{\bar{m}}{2\pi} & if \quad \bar{x} \leq 0 \\ \left(\tan^{-1}\left(\frac{\bar{y}}{\bar{x}}\right) + 2\pi\right) \cdot \frac{\bar{m}}{2\pi} & if \quad \bar{x} > 0, \ \bar{y} < 0 \end{cases} \quad (5)$$

The variability r of the mean date of occurrence around the average date is

$$r = \sqrt{\bar{x}^2 + \bar{y}^2} \text{ where } 0 \leq r \leq 1. \quad (6)$$

$r = 0$ corresponds to events being widely dispersed throughout the year, and r=1 to events occurring on the same day of the year.

2.5. PROBABILITY THEORY

The following sections are to a large degree an account of the L-moment approach to regional frequency analysis outlined in the influential work of Hosking and Wallis (1997), beginning with a note on probability theory.

Environmental data are often regarded as observations of random variables, generally denoted by X, and it is very rare that these values are equally likely to be observed (Hosking and Wallis, 1997). In probability theory, the relative frequency with which the values of X occur is described by its probability distribution. The cumulative distribution function,

$$F(x) = \Pr[X \leq x] \text{ where } 0 \leq F(x) \leq 1, \quad (7)$$

of a probability distribution describes the probability that the random variable, or observation, is lower than a specific value x. If $F(x)$ is a continuous function, which is often the case for environmental variables, it has an inverse function $x(F)$ called the quantile function of X. $x(p)$ is called the quantile of non-exceedance, given a probability p that X does not exceed the value $x(p)$. For example, the discharge of a river might have a probability p=1% of exceeding 100 m^3/s, which would then be the value of $x(0.01)$.

In frequency analysis, the object is to estimate the quantiles belonging to the distribution of the random variable of interest (Hosking and Wallis, 1997). The quantiles may also be expressed in terms of the return period, which is common in environmental and engineering practice. A quantile of return period T, X_T, is an observation, or event magnitude, that has the average probability $1/T$ of being exceeded by any single event. For annual data, an event magnitude with a return period of T years is equivalent to an annual non-exceedance probability

$$F(X_T) = 1 - 1/T, \quad (8)$$

and the magnitude of such an event is given by

$$X_T = x(1 - 1/T). \quad (9)$$

For engineering purposes, a return period of interest may be the design life of a structure, and thus the quantity X_T can be referred to as the design event. When flood and precipitation data are analyzed, the design event is called the design flood and design storm, respectively.

2.6. ESTIMATORS

To estimate the quantiles of the variable of interest, a distribution for the variable must first be known (Hosking and Wallis, 1997). It is common to assume that a suitable distribution can be defined apart from a set of unknown parameters. These usually include location and shape parameters, which are estimated from the observed data. A common measure of performance for the estimator $\hat{\theta}$ of parameter θ is the root mean square error (RMSE),

$$RMSE(\hat{\theta}) = \left\{E(\hat{\theta} - \theta)^2\right\}^{1/2}, \tag{10}$$

which has the same units as the parameter. A dimensionless measure, the relative RMSE, is obtained by the ratio of RMSE and θ.

2.7. MOMENTS

The moments of a probability distribution are used for describing its scale and shape (Hosking and Wallis, 1997). The first moment is the mean, the center location of the distribution and the expected value of a random variable X,

$$\mu = E(X). \tag{11}$$

Higher order moments are given by

$$\mu_r = E(X - \mu)^r \text{ with } r = 2, 3, \ldots \tag{12}$$

The second moment is the variance which measures the dispersion around the mean value,

$$\sigma^2 = \mu_2 = E(X - \mu)^2. \tag{13}$$

The coefficient of variation (CV) measures dispersion as a proportion of the mean,

$$C_V = \sigma/\mu, \tag{14}$$

and is a useful alternative to the variance. Estimating the shape of a distribution involves higher order moments, as for skewness and kurtosis. Skewness,

$$\gamma = \mu_3/\mu_2^{3/2}, \tag{15}$$

contains the third moment and measures whether the distribution is concentrated at the left and has a longer right tail (positive skew), or vice versa (negative skew). The forth moment is included in kurtosis,

$$\kappa = \mu_4/\mu_2^2, \tag{16}$$

which is related to the influence of extreme values on the variance, i.e. kurtosis increases as more of the variance is due to the presence of outliers (Westfall, 2014).

2.8. L-MOMENTS

Probability weighted moments (PWMs) were developed by Greenwood (1979) as an alternative to ordinary moments when estimating parameters to distributions whose inverse form are explicitly defined. However, the PWMs can only indirectly be interpreted as measures of scale and shape of a probability distribution. To overcome this, Hosking (1990) defined L-moments as linear combinations of the PWMs (the "L" refer to this fact, that they are linear combinations). L-moments have a good performance for small samples and computational simplicity compared to other estimation methods such as maximum likelihood, making them popular for applications to hydrologic extremes (Katz, 2002).

Analogous to ordinary moments, useful L-moments for summarizing data are the L-location (λ_1), which is the same as the mean of the distribution, and the L-moment ratios L-CV (τ), L-skewness (τ_3) and L-kurtosis (τ_4). The L-moment ratios are given by the formula

$$\tau_r = \lambda_r/\lambda_2 \text{ with } r = 3, 4, \ldots \quad (17)$$

where λ_2 is the scale measure L-scale. The L-moment ratios are therefore dimensionless. Sample L-moments are denoted l_r, and sample ratios by t_r. See Hosking and Wallis (1997) for detailed definitions.

The L-moment ratio diagram is a convenient way of comparing sample L-moment ratios with population values of frequency distributions (Hosking and Wallis, 1997). The values are plotted on a graph whose axes are L-skewness and L-kurtosis. Two-parameter distributions plot as points, and three-parameter distributions plot as lines, with different points on the line equivalent to different values of the shape parameter. For a homogenous region (see definition below), it is useful to plot the regional average L-moment ratios – average of at-site ratios in a region weighted by record length – to assess which distribution it resembles. In this way, the L-moment ratio diagram provides a visual assessment of the dispersion of the at-site L-moment ratios and can be used as a graphical tool to guide the selection of a suitable parent distribution in a regional frequency analysis.

2.9. REGIONAL FREQUENCY ANALYSIS

It is often a problem when estimating quantiles from annual data that record lengths are too short compared to the return period of interest (Hosking and Wallis, 1997). Generally, a record length at least as long as the return period is needed for reliable estimates, which seldom is the case for environmental observations.

Regional frequency analysis is a way to mitigate the problem of short records (Hosking and Wallis, 1997). It works by pooling together data from sites which are deemed similar enough, i.e. the at-site frequency distributions are approximately the same. In other words, a region is a group of sites whose observations are assumed to be drawn from the same distribution. Quantile estimates are then made from the larger dataset of the region, ideally with better accuracy than the at-site estimates.

The similarity of the at-site distributions is referred to as the homogeneity of the region, or heterogeneity if they are too dissimilar (Hosking and Wallis, 1997). A regional analysis involves assigning sites to regions, testing if the proposed regions are homogenous and finding suitable frequency distributions that fit the regional datasets.

2.9.1. Index flood method

One way to conduct a regional analysis is by the index flood method of Dalrymple (1960). As the name suggests, the method was developed for flood frequencies, but it can be used for any kind of data. It consists of two steps, where the first is to develop a dimensionless frequency curve, referred to as the regional growth curve in later works (e.g. by Schaefer, 1990; Hosking and Wallis, 1997; Di Baldassarre et al., 2006). The growth curve represents the ratio of an event magnitude of any frequency, i.e. the quantiles, to an index flood. The index flood is defined for each site in a region and commonly taken to be the at-site mean (Dalrymple, 1960). When applied to precipitation data, this is instead called the index storm.

The second step involves relating the index flood to some physical characteristic to enable the prediction of the index flood, and thus also the quantiles, at any point within a region. This makes it possible to assign any site with that characteristic to a frequency curve. Because of this, regionalization is a vital tool in the field of flood prediction at ungauged sites (Blöschl et al., 2013).

In the approach to the index flood method of Hosking and Wallis (1997), the index flood at site i is estimated by the sample mean of the data. The parameters of the at-site distributions are found by estimating L-moments from the sample data. The at-site estimates are combined in the regional average to give the parameters of the regional growth curve.

If $\hat{Q}_i(F)$ is the estimated quantile function of the frequency distribution for site i belonging to a homogenous region, then quantile estimates are calculated as

$$\widehat{Q}_i(F) = \hat{\mu}_i \hat{q}(F), \tag{18}$$

where $\hat{\mu}_i$ and $\hat{q}(F)$ are the estimated index flood and regional growth curve.

Given that the regional growth curve is correctly specified and that frequency distributions at different sites indeed are identical apart from a scale factor, the procedure of Hosking and Wallis (1997) assumes that observations are identically distributed, not serially dependent and that there is no cross-correlation between sites. Although these assumptions may not be exactly satisfied in practice, Hosking and Wallis argue the procedure to be appropriately robust to departures from the assumptions.

2.9.2. Identification of homogenous regions

A crucial step in regionalization is the identification of homogenous regions. There are numerous ways to delineate sites into regions and several involve subjective judgement. Hosking and Wallis (1997) argue that formation of regions should not be based on at-site statistics, but rather on site characteristics. These are, in principle, quantities that can be

known about a site without measurements having been carried out, such as location, elevation and other physical properties. Mean annual precipitation may also be considered as such a characteristic.

At-site statistics should instead be used in testing of homogeneity of a proposed set of regions (Hosking and Wallis, 1997). Otherwise, if for example L-CV is used for grouping, there would be a tendency to group together sites with high outliers, even though these outliers might be due to random fluctuations that happened to affect one site but not its neighbors.

2.9.3. Discordancy

The discordancy measure of Hosking and Wallis (1997) is used to identify sites which are inconsistent with a group of sites as a whole. This is measured by the at-site L-moment ratios and summarized in the discordancy measure D. The critical value of D, above which a site is considered discordant, is 3 for regions with 15 or more sites (D increases from 1.33 to 3 for 5 to 15 or more sites in a region). A site flagged as discordant should be scrutinized for errors in the data or put under consideration for removal from the region.

2.9.4. Homogeneity test

All sites in a homogenous region have equal population L-moment ratios, but due to sampling variability the at-site ratios will differ. The question is if the dispersion of the observed L-moment ratios is larger than what would be expected. The homogeneity test proposed by Hosking and Wallis (1997) compares the dispersion of at-site L-CV to the statistics of a homogenous region, obtained from Monte Carlo simulations. In the test, the flexible four-parameter Kappa distribution is fitted to the regional average L-moment ratios calculated from the sites (see appendix Eq. A26–A28). A large number of realizations are simulated with this distribution, with the same number of sites and record lengths as the samples. The simulation results are used to calculate the heterogeneity measure

$$H = \frac{(V-\mu_V)}{\sigma_V}, \tag{19}$$

where V is the weighted standard deviation of at-site sample L-CV, and μ_V and σ_V are the mean and standard deviation of simulated V. The region may be considered acceptably homogenous if $H \leq 1$, possibly heterogeneous for $1 \leq H \leq 2$, and definitely heterogeneous if $H \geq 2$.

It is also possible to use a heterogeneity measure based on L-skewness and L-kurtosis. Hosking and Wallis (1997) refer to this measure as V_3 and consider it appropriate for procedures based on hierarchical regions. Although, compared to the measure based on L-CV, they find that this measure lacks power to discriminate between homogenous and heterogeneous regions.

In this study, the H-statistic of the homogeneity test corresponding to V_3 is termed H_3 and the H-statistic based solely on L-CV is referred to as H_1. Unless specified otherwise, homogeneity refers to H_1.

2.9.5. Choice of regional frequency distribution

Hosking and Wallis (1997) suggest considering many families of distributions as candidates for a regional dataset. The set of distributions suggested by Hosking (2015) is able to adapt to a wide range of properties of the data, and comprises the generalized logistic, generalized extreme value, generalized Pareto, generalized normal, Pearson type III and the Gumbel distribution (see appendix for formulas).

Given a set of candidate distributions, a goodness-of-fit test may be used to asses which distribution gives the best fit to the data. The test for regional distributions of Hosking and Wallis (1997) is based on the notion that regional average L-moment ratios summarize the L-statistics of homogenous region. Given homogeneity, the scatter of at-site values in the L-moment ratio diagram should represent no more than sampling variability. The location and scale parameters of the distributions are estimated by the regional average mean (L-location) and L-CV. The test compares the differences between L-skewness and L-kurtosis of the fitted distributions, and the corresponding regional averages.

To assess the significance of the differences, simulations are used to calculate a sampling variability for the regional averages. The simulations are in principle the same as for the homogeneity test, and those computations can be used again here to calculate the standard deviation and bias of the regional averages. The goodness-of-fit measure Z reflects a fit acceptable at the 10% significance level for $|Z| \leq 1.64$. This assumes that Z has a standard normal distribution, which is only accurate if the region is perfectly homogenous and if there is no serial correlation or cross-correlation present in the data. Should several distributions be found to be acceptable, their growth curves can be compared. If these are approximately equal, then any of the distributions is adequate.

2.9.6. Estimation of a regional frequency distribution and its accuracy

In the L-moment procedure of Hosking and Wallis (1997), a regional frequency distribution is fitted by equating the L-moment ratios of a suitable distribution to the regional averages calculated from the samples. For three-parameter distributions, sample L-moment ratios t, t_3 and t_4 are computed and used to estimate the regional quantile function $\hat{q}(F)$. Since the quantile estimates for each site is scaled by the index flood, the regional average mean, l_1^R, is set to 1. Estimate of quantile with non-exceedance probability F at site i is calculated as

$$\widehat{Q}_i(F) = l_1^{(i)} \hat{q}(F). \tag{20}$$

The accuracy of the quantile estimates can be assessed in Monte Carlo simulations of a synthetic region that matches the region used for the estimates in terms of heterogeneity and intersite dependence. Variation of the at-site L-CV in the synthetic region is chosen to match the observed H_1-value. A correlation matrix can be used to describe the observed correlation pattern of the data, but if no specific pattern is discernible between the sites, they can be assumed to be equicorrelated. The average cross-correlation between all sites is then used. A large number of realizations of the synthetic region are made with the

same number of sites, record lengths and regional distribution as the region used for estimates. A relative RMSE of the quantiles may be computed from the simulations. An interval around the estimated growth curve can also be calculated, within which a given ratio of simulated values fall. This is referred to as error bounds in Hosking and Wallis (1997).

3. DATA AND METHODS

3.1. DATABASE

The database used in this study was created involving the work of researchers at the University of Trento. The software DB Browser for SQLite (v. 3.9.1) was used to extract data from the database.

The database contains hydrological and meteorological time series data as well as spatial information of the Adige basin. Precipitation and discharge data were available in daily, hourly and sub-hourly (5 min, 10 min and 30 min) time series. However, the majority of hourly and sub-hourly series were initiated after the year 2000 and no sub-daily series extended further back than 1977. Availability of daily data were better, with records going as far back as the 1920s. The most recent records end in early 2015, and roughly half of all records end before 2010. There were also historic records of monthly series which were not considered in this study.

Based on the availability of data records (summarized in Table 1) it was decided that a suitable study period would be the 40-year period 1975-2014. It was also decided that the focus should be on daily data and that sub-daily records could be included after aggregation into daily series.

Table 1. Number of available records in database and summary of record lengths.

Variable	Available records	Mean (yrs)	Min (yrs)	Max (yrs)	Std. (yrs)
Precipitation	643	29	0.02	94	29
Discharge	128	18	0.01	89	19

3.2. PROCEDURE FOR DEVELOPING ANNUAL MAXIMUM SERIES

The extracted time series were tested to assess if they were suitable for developing AMAX series. Primarily, the years used in the AMAX series should not have too many missing values, otherwise it is plausible that the maximum value that year was not recorded. The main idea in the implemented selection procedure was to use the information in the seasonality of annual maxima, together with a threshold for missing values. The steps are explained in detail below and were performed in MATLAB (v. 2017b). Selected records are summarized in Table 2.

1. First, every time series (daily and sub-daily) for precipitation and discharge sites with more than 15 years between the reported start and end dates were extracted as csv-files from the database.
2. For each time series, the years in the period 1975-2014 with less than 5% missing values were selected. This threshold was included to get a reliable first estimate of the seasonality indices.
3. Sub-daily series were then aggregated to daily series. For precipitation series, this meant finding the sum of values recorded over 24 hours. However, there seemed to be some inconsistencies in the database regarding which 24 h-period was defined as a day. For several sites, both daily and sub-daily series were available, which allowed for comparisons between the aggregated daily series and the database counterparts. For 10 min-data, values were summed between 9 a.m. the first day to 9 a.m. the following day (the date of the second day was assigned to the value). Although there were examples of 5 min-series where summing between midnight to midnight or 10 a.m. to 10 a.m. yielded values closer to the database daily series, 9 a.m. to 9 a.m. was more common and thus used for all series. For 60 min data, sums between 10 a.m. to 10 a.m. gave values most similar to the database daily series. In the case of discharge data, the mean value was calculated for each day, defined as midnight to midnight.
4. To construct AMAX series, the largest daily event was selected for each hydrological year among the selected calendar years. The hydrological year was defined as October 1 to September 30 the following calendar year. The resulting series were checked so that no two maxima occurred within one week, to ensure that they were not generated by the same storm event, i.e. to minimize serial correlation.
5. The seasonality of each AMAX series was then analyzed to find the mean date of occurrence, D_{mean}, and its variability, r.
6. The information from the seasonality analysis was used for a more rigorous selection criterion. The extracted time series were tested one more time. For each series, a window was defined as +/-10 days/r around D_{mean}, i.e. the size of the window was inversely proportional to the variability of the mean date of occurrence ($0 \leq r \leq 1$). The average window size was +/-26 days for precipitation and +/-20 days for discharge. Years with less than 0.05% missing values within the window were considered to have complete records. Time series with at least 20 complete years were selected.
7. Steps 3–5 were repeated for time series selected in step 6 to construct the AMAX series used in further analysis. In the case where daily and aggregated sub-daily series both met the criteria in step 6, the daily series were chosen since these tended to have longer records and this minimized the uncertainty introduced by the aggregation. Before generating the final AMAX series, it was checked in GIS software that only sites located within the Adige basin were used.

Table 2. Number of selected records and summary of their record lengths.

Variable	Selected records	Mean (yrs)	Min (yrs)	Max (yrs)	Std. (yrs)
Precipitation	84	32	21	39	5.5
Discharge	17	31	20	39	5.7

3.3. CATCHMENT DELINEATION

Discharge time series were available in units of m^3/s and converted to mm/d in the AMAX series in accordance with precipitation data. The specific discharge, i.e. the value in m^3/s divided by sub-catchment area in m^2, was calculated for each discharge site and then transformed from m/s to mm/d. This scaling affects L-location but not L-CV and higher order L-moment ratios.

The Adige basin at the city of Trento and its sub-catchments were delineated using the digital elevation model Global Multi-resolution Terrain Elevation Data 2010 (GMTED2010) from the U.S. Geological Survey and the National Geospatial-Intelligence Agency (U.S. Geological Survey, 2015). The spatial resolution used was 7.5 arc-seconds. Delineation was performed in QGIS (v. 2.18.7) with the SAGA (v. 2.3.2) algorithms *Fill sinks*, *Strahler order*, *Channel network and drainage basins* and *Upslope area*.

3.4. SCREENING OF DATA

Time series in the database were labelled with a quality assessment. Each value in the time series was associated with one of 53 different quality codes. These codes were grouped into *flag* equal to 0 or 1. Data with *flag*=0 were described as *missing*, *incomplete* or *suspect*, whereas data with *flag*=1 contained descriptions such as *good* or *complete*, but also *unverified* or *interpolated from hydrological records of the Italian Hydrological Service*. Test results for L-moments were first generated including all available data. An examination of suspicious outliers showed that these all belonged to data with *flag*=0.

All data with *flag*=1 was included in this study. While the inclusion of unverified data introduced uncertainty, the trade-off for longer records was deemed necessary. As an example, precipitation site 90269 was found to have 34 complete years but would lose 16 years of available data in the study period if unverified data were excluded. Overall, the assessment is that unverified data represents a minority of analyzed data.

The lag-one serial correlation coefficient was computed for the AMAX series. Precipitation sites had an average value of 0.024, with a standard deviation of 0.17. For discharge, the values were -0.09 and 0.14, respectively.

3.5. STUDY AREA

The Adige river is the second longest river in Italy (Encyclopædia Britannica, 1998). It rises from mountain lakes below the Resia pass in the north-eastern Italian Alps and flows south and east to Bolzano where is joins with the Isarco River. Past Bolzano it flows south through the Lagarina Valley passing Trento, the capital of the Trentino-Alto Adige region.

The drainage area of the Adige at Trento is 9,800 km^2. It is a mountainous region, with the highest peaks predominantly in the western part and at the northern edge along the Austrian border (Figure 1). The low-lying river valley is mainly oriented in the north-south direction.

Mean annual precipitation varies between 500 and 1,260 mm with an average of 830 mm. The main direction of storms is from the south and west during autumn, and the catchment response time is approximately 20 h (Manfreda and Fiorentino, 2008). This response time makes the analysis of daily data suitable for detecting the largest flood peaks.

The river is modified by human action, with dikes built on both its sides in its path through the valley (Alkema et al., 2003), and the main river and its tributaries being exploited for hydroelectric power generation. Dams in use today were built before the 1960s (Zolezzi et al., 2009) and the locations of the 25 reservoirs are marked in Figure 1.

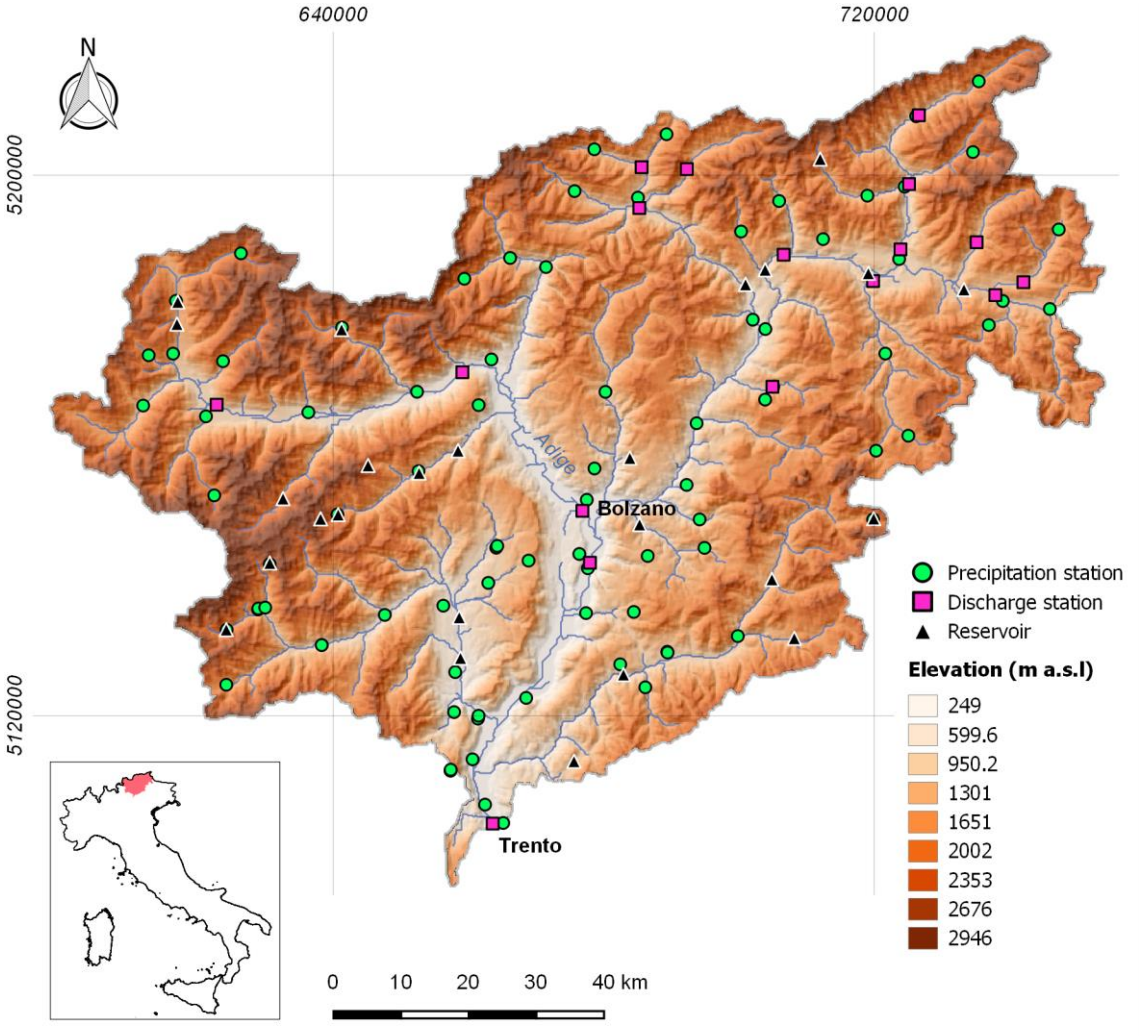

Figure 1. Map of the Adige basin down to Trento showing elevation. Locations of selected precipitation (circles) and discharge (squares) sites are plotted, together with reservoirs (triangles) in the river network. Coordinate system WGS 84/UTM zone 32N, EPSG: 32632. Coordinates in decimals.

3.6. L-MOMENT AND REGIONAL ANALYSIS METHODOLOGY

The development and analysis of L-moments and the regional frequency analysis were performed in R (v. 3.4.2), with the packages *lmom* (Hosking, 2015) and *lmomRFA* (Hosking, 2017).

3.7. TREND ANALYSIS AND SEASONALITY ANALYSIS METHODOLOGY

Trend analysis of AMAX series were performed in R with the packages *data.table* (Dowle et al, 2017), and *modifiedmk* (Patakamuri, 2017).

A sensitivity analysis was performed to examine the influence of gaps (i.e. missing years) in the AMAX series on the detection of significant trends.

1. First, AMAX series with no missing years were selected and the sensitivity test was performed on this set of series.
2. A percentage of the AMAX values was randomly removed from each series, and the MK trend test was then performed on these series with artificial gaps.
3. The test was repeated with 5%, 10%, 15%, 20% and 25% of AMAX values removed. For each percentage of artificial gaps, the number of significant trends was stored.
4. Since the algorithm involved the generation of random numbers, it was implemented with a Monte Carlo procedure. For each percentage of artificial gaps, results were averaged over 1000 outcomes of the algorithm.
5. Finally, the difference between the results with artificial gaps and the original series, i.e. with no artificial gaps, was compared to assess the reliability of trend results for series which contained gaps.

Calculations of β-values (Eq. 1) for the trend analysis of mean date of occurrence, as well as the seasonality analysis, were implemented in MATLAB (v. 2017b).

4. RESULTS

Results are summarized in the following sections. See Tables A1 and A2 in appendix for detailed results for each site.

4.1. TREND ANALYSIS OF ANNUAL MAXIMUM SERIES

The MK trend analyses of the AMAX series performed at 10%, 5% and 1% significance levels displayed a pattern where a minority of sites exhibited predominantly negative trends (Table 3). The percentages of AMAX series with significant negative trends were larger than the significance levels, with the exception of precipitation series at the 5% level. There, 4 out of 84 series (4.8%) showed significant negative trends. Record lengths of AMAX series with significant trends at the 1% level were all above 30 years.

All AMAX series were included in the data summary in Figure 2, but for the estimation of distributions, series with significant trends at the 5% level were excluded.

Table 3. Trend analysis of annual maximum series for selected significance levels, with number of significant positive (+) and negative (-) trends for each variable and the number of samples (n).

Variable	Significance level		
	10%	5%	1%
Precipitation (n=84)			
+	2	2	0
-	11	4	3
Discharge (n=17)			
+	0	0	0
-	5	3	2

4.1.1. Sensitivity analysis

36 out of the 84 precipitation AMAX series, and 10 out of 17 discharge series, were found to have no missing years and where thus used in the sensitivity analysis. The number of significant trends decreased when artificial gaps were introduced, and the number generally decreased more for larger gaps (Table 4 and 5).

Furthermore, the p-values for each site were averaged over the outcomes of the Monte Carlo simulations performed for each percentage of artificial gaps. This analysis showed that no site developed significant trends with increasing gaps, but rather the opposite: the average p-values increased with increasing artificial gaps for the sites that had significant trends when no artificial gaps had been introduced, leading to sites losing significance as the artificial gaps increased (Table A3 and A4 in appendix).

Table 4. Sensitivity analysis of precipitation trend results, with number of significant positive (+) and negative (-) trends with different percentages of AMAX values randomly removed (artificial gaps). Analysis performed on a subsample of 36 series which had no gaps in record. Note that the significant numbers of trends are 3.6, 1.8 and 0.36 for the 10%, 5% and 1% significance levels respectively. Results are based on 1000 realizations of the algorithm. Trend results for the 36 series with no years removed (0% artificial gaps) are included for comparison.

Artificial gaps	Trend	Significance level		
		10%	5%	1%
0%	+	1	1	0
	-	4	2	1
5%	+	1.2	1.0	0
	-	3.4	1.6	0.5
10%	+	1.5	0.9	0
	-	3.3	1.5	0.3
15%	+	1.5	0.8	0
	-	3.1	1.4	0.3
20%	+	1.6	0.8	0
	-	3	1.3	0.2
25%	+	1.6	0.8	0
	-	2.9	1.2	0.1

Table 5. Sensitivity analysis of discharge trend results, with number of significant positive (+) and negative (-) trends with different percentages of AMAX values randomly removed (artificial gaps). Analysis performed on a subsample of 10 series which had no gaps in record. Note that the significant numbers of trends are 1, 0.5 and 0.1 for the 10%, 5% and 1% significance levels respectively. Results are based on 1000 realizations of the algorithm. Trend results for the 10 series with no years removed (0% artificial gaps) are included for comparison.

Artificial gaps	Trend	Significance level		
		10%	5%	1%
0%	+	0	0	0
	-	3	2	1
5%	+	0	0	0
	-	2.4	1.4	0.3
10%	+	0	0	0
	-	2.2	1.3	0.3
15%	+	0	0	0
	-	2.0	1.1	0.2
20%	+	0	0	0
	-	1.7	0.9	0.2
25%	+	0	0	0
	-	1.5	0.8	0.1

4.2. L-MOMENTS SUMMARY

The spatial distributions of L-location, L-CV and L-skewness are summarized in Figure 2. Both color and size of symbols reflect the magnitude of values, where the smallest and largest symbols belong to the sites with the lowest and highest values, respectively. The precipitation L-moment values were typically higher in the central part of the basin. For discharge, the L-location and L-skewness were mainly higher for sites belonging to the smaller sub-catchments in the northern part of the basin. Beyond this, other geographic patterns are difficult to discern.

For discharge, the L-moment ratio diagram (Figure 3) revealed that the regional average had the best agreement with the generalized normal (GNO) distribution. In the case of precipitation, the regional average was closest the line of Pearson type III (PE3), but also near the generalized normal, generalized extreme value (GEV) and Gumbel (G) distributions (Figure 4). In both cases, the scatter of sample points covers the set of distributions.

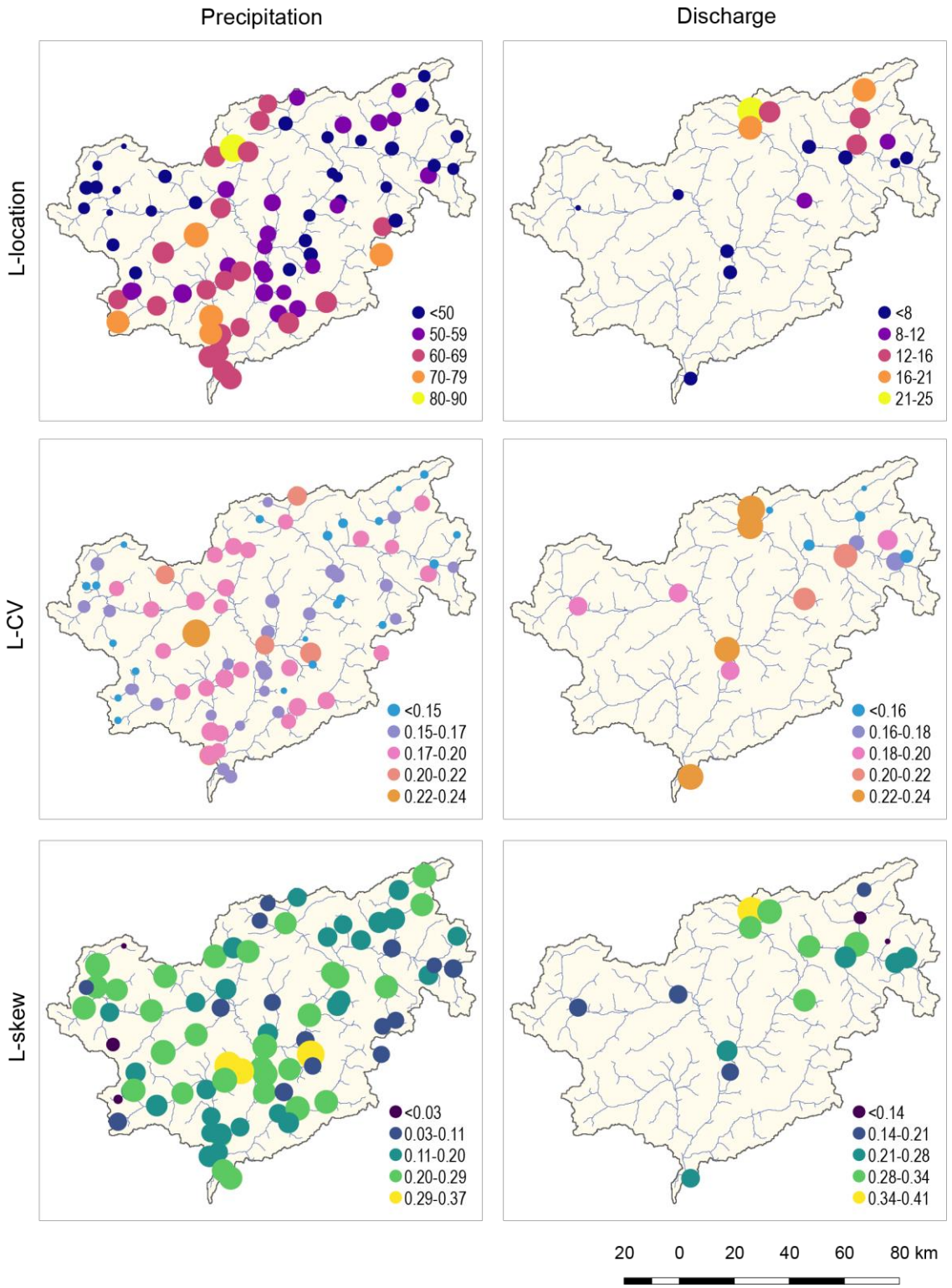

Figure 2. At-site values of L-location (1st row), L-CV (2nd row) and L-skewness (3rd row) for precipitation (left column) and discharge (right column) sites. Symbol size increase with increasing values. Values are color-categorised in five levels according to magnitude (see legends). Units of L-location are mm/d.

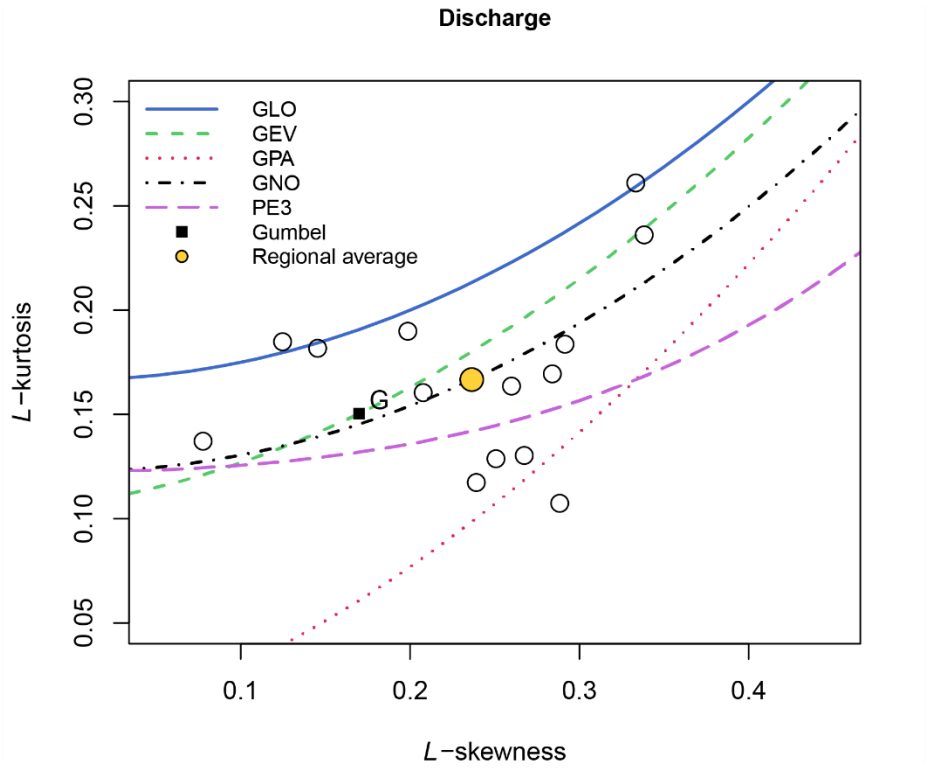

Figure 3. L-moment ratio diagram for discharge comparing sample L-kurtosis and L-skewness (hollow circles) and the regional average (filled circle) to values of the frequency distributions generalized logistic (GLO), generalized extreme value (GEV), generalized Pareto (GPA), generalized normal (GNO), Pearson type III (PE3) and Gumbel (G).

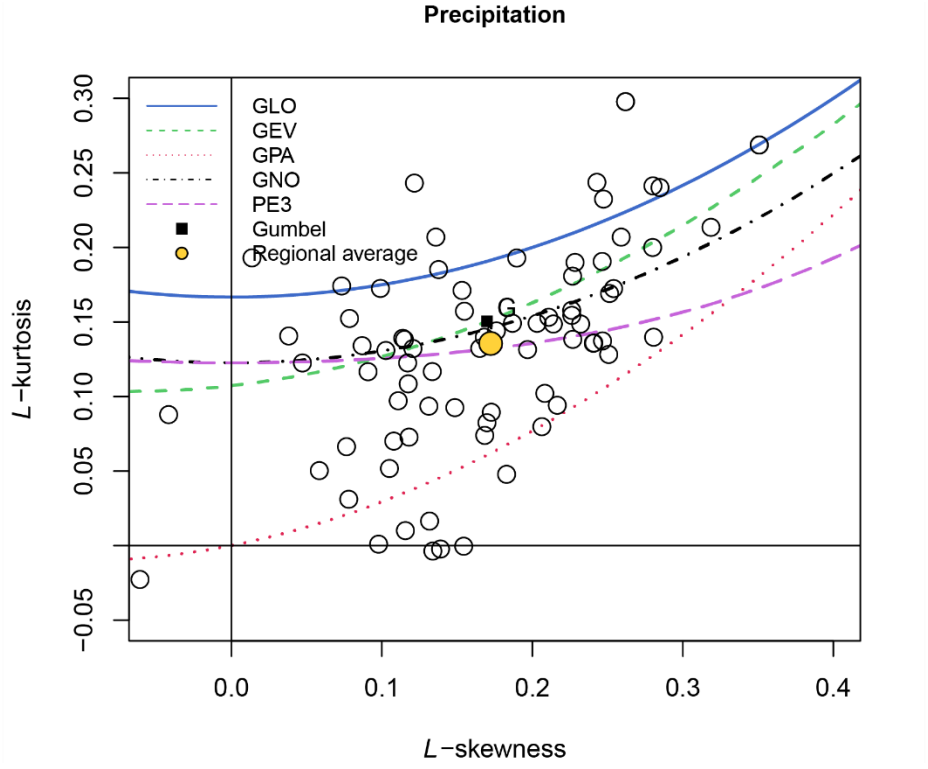

Figure 4. L-moment ratio diagram for precipitation. See description for Figure 3.

4.3. DISCORDANCY TEST

Two precipitation series were found to be discordant, with *D* larger than the critical value 3.0, which warranted these series to be checked for potential errors. The first series, belonging to site 90104, had unverified values for the years 1975-1980, and subsequently verified data quality from 1981 to 2013. The annual maxima of 1975-1980 were in good agreement with the rest of the period. The reason for discordancy was the high L-CV of this series, likely caused by the extreme value in 1999 of 190 mm/d, which was the highest measured at any site. The second series, from site 90014, had the smallest maximum value of all series, and all values in the time series were verified apart from a short interval in March 2013. Based on this, neither series was excluded. No discharge series was found to be discordant.

4.4. REGIONAL HOMOGENEITY

The heterogeneity measure of Hosking and Wallis (1997) was used to assess whether the sites in the study area could be treated as a single homogenous region. The region was considered acceptably homogenous for $H \leq 1$, possibly heterogeneous for $1 \leq H \leq 2$ and definitely heterogeneous for $H \geq 2$. With 10 000 realizations of the algorithm, the values of H_1 were found to be 0.27 for precipitation and 1.50 for discharge, with similar magnitudes for H_3. (Table 6). In other words, the whole basin was homogenous with respect to precipitation but possibly not for discharge. Therefore, only precipitation data were considered in the regional frequency analysis.

Table 6. Heterogeneity test statistics. H_1 is based on L-CV and H_3 on L-skewness and L-kurtosis.

Variable	H_1	H_3
Precipitation	0.27	-0.28
Discharge	1.50	-1.86

4.5. REGIONAL FREQUENCY ANALYSIS

A more formal way of identifying suitable frequency distributions than inspection of L-moment ratio diagrams is to use the goodness-of-fit test described in section 2.9.5. Both PE3 and the GNO distributions had acceptable fits (Table 7). Growth curves for the distributions were compared and found to be approximately equal. Both distributions may be adequate, but PE3 was selected for quantile estimates on account of the lower *Z*-value. The Gumbel distribution was not tested, as it was not included in the R-package. But judging from the relative distances to the regional average in Figure 4, Gumbel should have a Z-value very similar to GEV.

Table 7. Test statistics for goodness-of-fit test. The fit is considered acceptable if $|Z|$ is less than 1.64.

Distribution	Z
GLO	7.30
GEV	2.03
GNO	1.32
PE3	-0.50
GPA	-9.72

The regional frequency distribution was fitted by the method of L-moments. The population L-moments of the region were equated to the regional average L-moment ratios from the sample data (Table 8).

Table 8. Regional average L-location (l_1), L-CV (t), L-skewness (t_3) and L-kurtosis (t_4).

l_1^R	t^R	t_3^R	t_4^R
1	0.166	0.172	0.136

The PE3 distribution was parametrized by the conventional moments mean μ, standard deviation σ, and skewness γ. These parameters were estimated from the regional L-moments (Table 9). Expressions for the L-moments in terms of parameters of PE3 and remaining distributions may be found in Hosking and Wallis (1997).

Table 9. Fitted parameters for regional Pearson type III distribution.

Distribution	μ	σ	γ
PE3	1	0.305	1.045

Monte Carlo simulations were used to assess the accuracy of the quantile estimates from the fitted regional distribution, accounting for heterogeneity and inter-site dependency. The variation of the at-site L-CV in the simulated region was set to the L-CV range of the samples, divided by 4.1 in order to match the observed H_1=0.27. Sites were assumed to be equicorrelated. The average cross-correlation was calculated as 0.360 and included in the simulations.

The estimated regional growth curve of the region with 90% error bounds is plotted in Figure 5 and summarized for selected values of non-exceedance probabilities F in Table 10. The index storm is scaled by the growth curve to give at-site quantile estimates. An event with a return period of 100-years (F=0.99) was estimated to be up to twice the magnitude of the index storm.

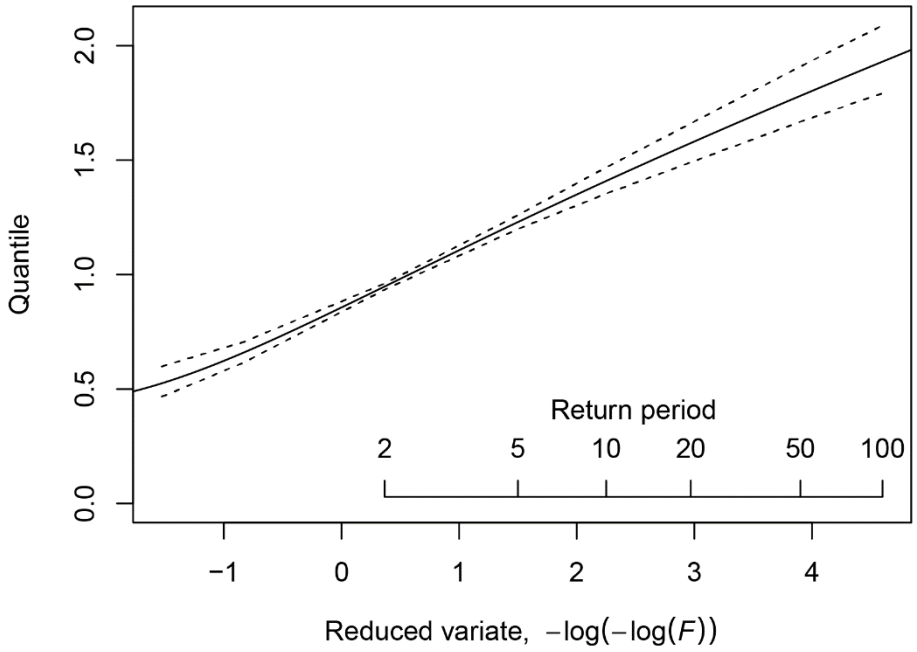

Figure 5. Regional growth curve for precipitation with 90% error bounds (dashed lines) for return periods up to 100-years.

Table 10. Regional quantile estimates $\hat{q}(F)$ with regional average RMSE and 90% error bounds (lower and upper) for selected non-exceedence probabilities F. Results based on 10 000 realizations.

F	$\hat{q}(F)$	RMSE	Lower bound (0.05)	Upper bound (0.95)
0.01	0.53	0.03	0.48	0.59
0.50	0.95	0.01	0.94	0.96
0.80	1.23	0.01	1.21	1.25
0.90	1.41	0.03	1.36	1.46
0.98	1.78	0.06	1.68	1.89
0.99	1.93	0.08	1.81	2.07

Event magnitudes with return periods of up to 100 years were estimated for annual maximum precipitation at site 90462 located just outside Trento, using Eq. 20 and the index storm of 66.7 mm/d (Table 11). The quantile estimate for the site had an upper bound of 147.6 mm/d for the 100-year storm. The time series showed that a similar amount, 134 mm, fell over January 31– February 1 in 1986. This did not coincide with a notable increase in the series of the nearby discharge site 90415 in Trento.

Table 11. Estimated annual maximum precipitation $\hat{Q}(F)$ at site 90462 on the outskirts of Trento for return periods of up to 100 years. Results represent regional quantile estimates and error metrics in Table 8 scaled by the index storm.

Return period (yrs)	F	$\hat{Q}(F)$ (mm/d)	RMSE (mm/d)	Lower bound (0.05) (mm/d)	Upper bound (0.95) (mm/d)
1	0.01	35.0	2.9	30.7	40.4
2	0.50	63.2	4.2	56.6	70.4
5	0.80	82.0	5.6	73.4	91.9
10	0.90	94.0	6.6	83.9	105.8
50	0.98	118.9	9.1	105.2	135.4
100	0.99	128.8	10.2	113.7	147.6

4.6. L-MOMENTS AND MEAN ANNUAL PRECIPITATION

A visual inspection of the relationship between sample L-CV and MAP (Figures 6), as well as L-skewness and MAP (Figure 7), gives some indication of a decrease of the L-moments with increasing MAP. When the relationship was formalized by fitting a linear model to the data, it was in both cases very weak (adjusted $R^2=3.1\cdot10^{-3}$ for L-CV and $2.4\cdot10^{-2}$ for L-skewness) and only significant at a 10% level for L-skewness (p-value=0.27 for L-CV and 0.09 for L-skewness). The slope was in both cases negative.

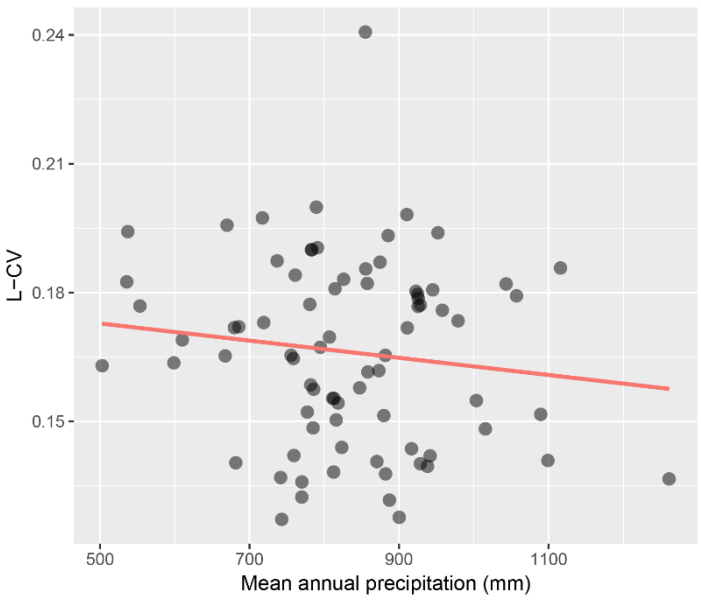

Figure 6. Sample L-CV of precipitation plotted against mean annual precipitation. Line represents linear regression model ($R^2=3.1\cdot10^{-3}$, p-value=0.27).

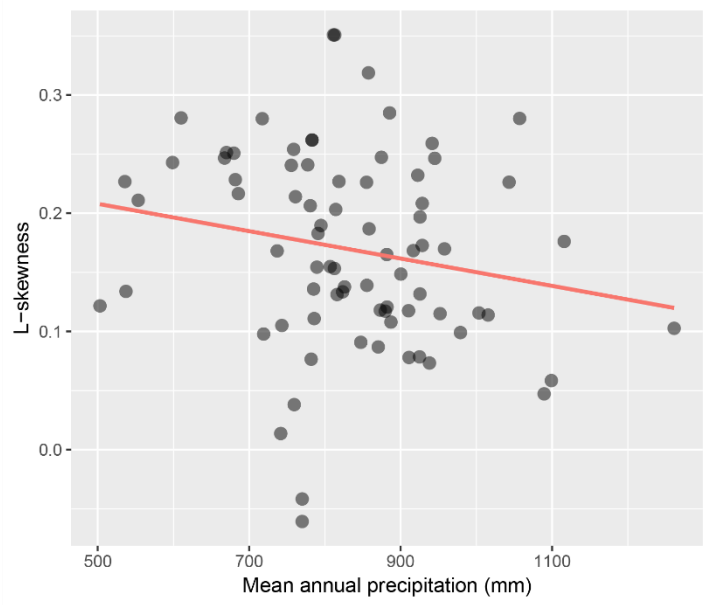

Figure 7. Sample L-skewness of precipitation plotted against mean annual precipitation. Line represents linear regression model (R^2=2.4·10^{-2}, p-value=0.09).

4.7. SEASONALITY ANALYSIS

The findings of the seasonality analysis are summarized for precipitation in Figures 8 and for discharge in Figure 9, where the color and direction of arrows represent the mean timing D_{mean} of annual maxima at each site (a D_{mean} of January 1 would point north and have an angular value of 0). The length of the arrows is proportional to the variability *r*, where longer arrows mean lower variability.

The analysis showed that the precipitation extremes were characterized mainly by autumn storms, with D_{mean} in August and September being most common. The seasonality was however rather weak, with a mean value of 0.45 and standard deviation of 0.13 for *r* and a range of July-November for D_{mean}. Looking at the spatial distribution, there seemed to be a pattern of earlier maxima occurring in the eastern part of the basin, and later maxima being more common in the western part.

The seasonality was stronger for floods, where *r* had a mean value of 0.70 and a standard deviation of 0.16. D_{mean} occurred in summer, predominantly in July, indicating that the timing of discharge extremes typically preceded precipitation extremes.

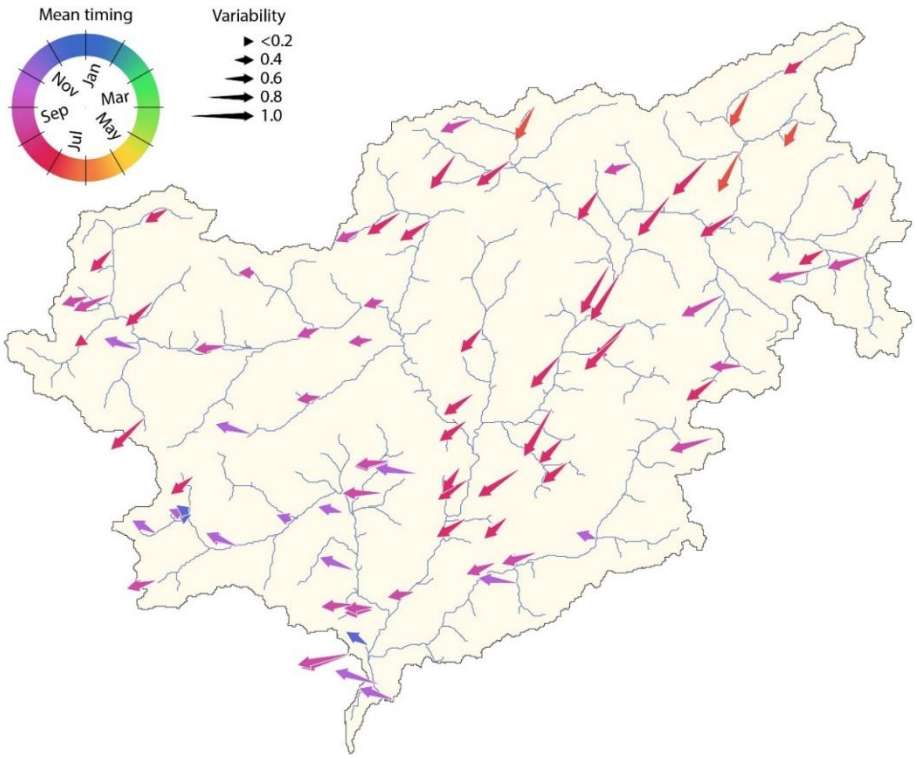

Figure 8. Seasonality for precipitation extremes. Arrow color and direction indicate mean timing of extremes. Arrow length is proportional to variability of timing.

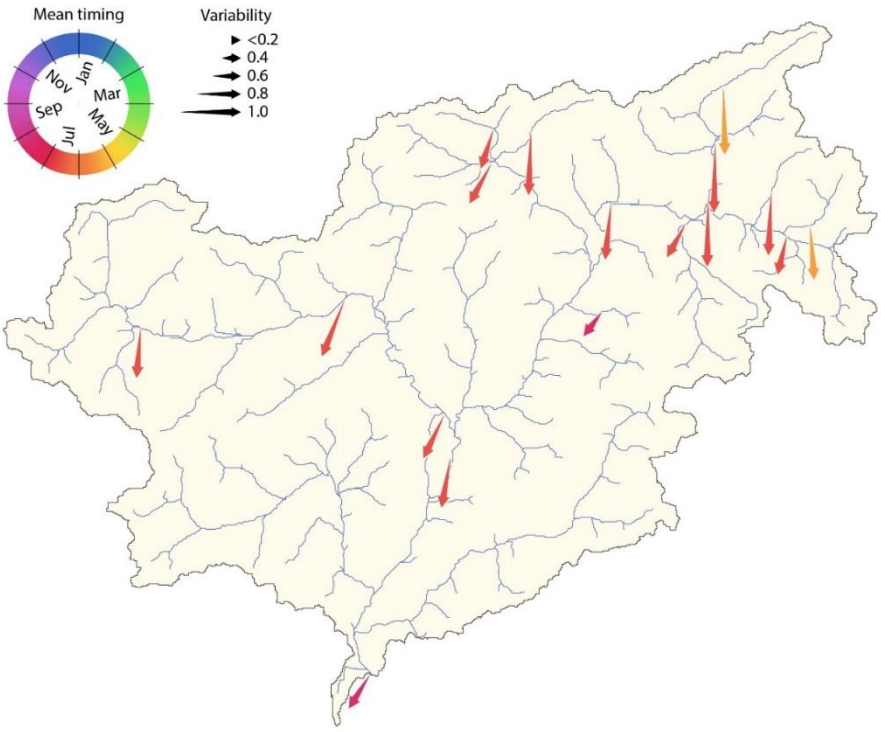

Figure 9. Seasonality for discharge extremes. See description of Figure 8.

A more detailed view of the seasonality may be obtained by the monthly distributions of AMAX occurrences. Figure 10 shows that both precipitation and discharge maxima were characterized by a single annual peak, roughly corresponding to the most common values of D_{mean}. The distribution peak was more pronounced for discharge, which reflected the larger values of r. The distribution also revealed that AMAX values of discharge started in May, were most common during June and July, and occurred to a lesser extent throughout autumn. Only a few values were recorded in the period December–April. For precipitation, AMAX values occurred during all parts of the year, but were most common during autumn.

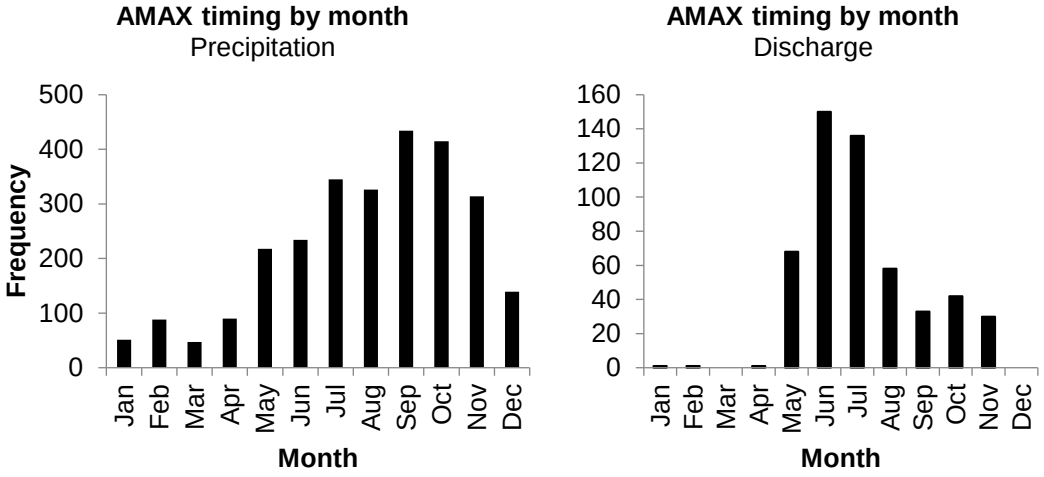

Figure 10. Number of AMAX occurrences in each month for precipitation (left) and discharge (right).

4.7.1. Trends in timing of maxima

An estimate of the Theil-Sen slope was performed on the dates of annual maxima of each individual series. The trend estimators β for all series are summarized in boxplots in Figure 11. Positive β-values represent a trend toward later dates whereas negative values indicate a shift to earlier dates.

The result suggests a small shift toward later floods. The median β-value of +2.2 days/decade for discharge translates to less than 10 days over the whole 40-year period. For precipitation, the values are quite evenly spread around the median of +0.6 days/decade and give no clear indication of a shift in the timing of maxima. However, the variability of precipitation β-values was greater than for discharge.

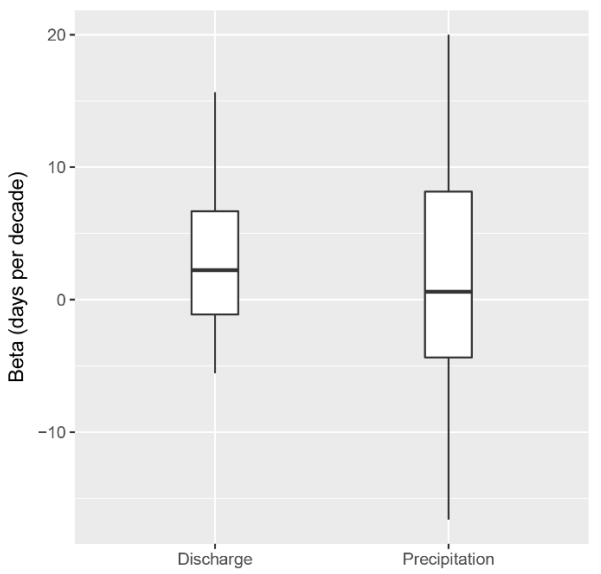

Figure 11. Boxplot summarizing the β-values of Theil-Sen slopes for occurrence dates of annual maxima. Unit of β is days per decade.

5. DISCUSSION

5.1. TREND ANALYSIS OF ANNUAL MAXIMUM SERIES

Overall, the percentages of AMAX series with significant trends were consistently larger than the significance levels, i.e. larger than we expect to be explained by randomness. While the percentage of precipitation AMAX series was just under the 5% level, the conclusion was still that the null hypothesis of no change could be rejected. A weak but significant signal of decreasing extremes was thus observed in the study period.

No information has been found indicating that any reservoirs were constructed during the study period, so this should not have influenced the trend analysis of discharge series. The number of analyzed discharge AMAX series was however low and a larger sample would be necessary to draw more confident conclusions about the basin as a whole.

Regarding precipitation trends, a study by Crisci et al. (2002) of the Tuscany region in Italy observed that significant trends in 1970–1994 were predominantly positive: 13 series of AMAX daily precipitation were found to be positive at a 5% significance level, and 1 to be negative, out of a sample size of 81.

On the global scale, studies of long-term observational records of precipitation show a tendency towards an increase in extremes, although there are regional differences, and compared to other climatic indices the precipitation indices show less large-scale significance. (Alexander et al., 2006). Analyzing a global dataset of daily precipitation extremes from 8326 sites with records spanning 1900-2009, Westra et al. (2013) found that two thirds of the observed significant trends were positive and one third were negative. However, only positive trends were statistically significantly different from the null hypothesis of no trend.

Since the results of a trend analysis depend on the observational window it would be interesting to investigate a longer study period. It would also be interesting to compare results with other mountainous regions. A model study of orographic precipitation extremes has suggested that mountainous regions respond differently to climate change and might experience less of an increase in precipitation extremes than is expected elsewhere (Siler and Roe, 2014).

5.1.1. Sensitivity analysis

Results discussed in the above section also hold for the subsamples with complete years of record, i.e. percentage of sites with significant trends were larger than the significance levels also for the 36 precipitation sites and 10 discharge sites (see results for 0% artificial gaps in Table 4 and 5). The question was then if the sensitivity analysis supported the inclusion of the remaining sites which contained gaps.

Fewer trends were detected when more data was removed from the subset of AMAX series with only consecutive annual values. Also considering that the average p-values of individual sites showed that increasing gaps only lead to loss of trends, these results seemed to indicate that trends were harder to detect when data were missing. This could mean that the number of significant trends for the series containing gaps have, if anything, been underestimated.

The presence of gaps in the AMAX series means there is information missing, and trend results for such sites are thus uncertain. However, the sensitivity analysis performed here did lend support to the findings of the trend analysis, and the conclusion was that all available series could be included.

5.2. L-MOMENTS SUMMARY

The dominant storm direction from the south to the northeast during autumn roughly corresponded with the spatial distribution of precipitation L-moments in Figure 2, which is in line with the results from the seasonality analysis of rainfall maxima being most common during this part of the year.

The specific discharge maxima tended to be higher in the smaller subcatchments of the basin. Flood peaks scaled by catchment area have been shown to decrease with increased catchment area (Eaton et al., 2002), as it is less likely for larger catchments that rainstorms cover the whole area and that they will be fully saturated (Viglione et al., 2010). Although, since only daily data have been analyzed, many of the observed discharge peaks may have been induced by long-rain events which tend to be uniformly distributed over large areas.

It was beyond the scope of this study to quantify relationships between extremes and physical processes, but of course, spatial differences in the distributional properties may be explained by site characteristics such as land use, soil permeability, mean catchment elevation etc. The exception is mean annual precipitation, which is discussed further below.

5.3. REGIONAL HOMOGENEITY

The discharge data were found to be possibly heterogeneous. Then, the regional average in the L-moment ratio diagram is likely not representative of the data since the samples may belong to different distributions. However, even with some degree of heterogeneity it could still be the case that quantile estimates from a regional analysis are more accurate than at-site estimates (Hosking and Wallis, 1997). Such a comparison has not been performed here.

It should be noted that an examination of site characteristics might reveal that there is no apparent physical reason to subdivide the discharge sites into smaller regions. If heterogeneity in this case is caused by a few outlying sites, Hosking and Wallis (1997) recommend that the physical argument rather than the statistical should be emphasized, and that the homogeneity of the region may be masked by sampling variability of the data. In other words, homogeneity cannot be entirely written off without such an examination.

Results are also indeterminate for discharge homogeneity measured by shape parameters, with H_3 in the possibly heterogeneous range. This casts doubt about the adequacy of the larger Triveneto region as a homogenous macro-region in the VA.PI. procedure. Nor does the assumption of Manfreda and Fiorentino (2008), that discharge in the Adige basin is homogenous with respect to L-CV, find much support in the results. Rather, they are in line with Persiano et al. (2016), who find the Triveneto region to be heterogeneous. Of course, inferences from the Adige basin to the wider Triveneto region are difficult to make, but the share of sites located in the Adige basin used by Persiano et al. – roughly half – was regarded large enough to draw these parallels.

Precipitation maxima were found to be homogenous. Since daily durations have been analyzed, the maxima may be related mainly to large scale storms compared to the size of the basin, as mentioned above. Considering this, it is perhaps expected of the precipitation maxima to show this degree of homogeneity.

Castellarin et al. (2008) examined effect of cross-correlation on the homogeneity test of Hosking and Wallis. With Monte Carlosimulations of 30 sites with up to 50 years of record, their results for a cross-correlated region indicated that observed *H*-values in the 0-1 range correspond to *H*-values in the 1-2 range for an uncorrelated region. They considered an equicorrelated region with cross-correlation equal to 0.4. Since average cross-correlation for precipitation maxima in this study was found to be 0.36, it is possible that the region was falsely identified as homogenous.

5.4. REGIONAL FREQUENCY ANALYSIS

The Pearson type III and generalized normal distributions were found to be consistent with the data for precipitation extremes. However, since a degree of serial correlation and cross-correlation is present in the data, the estimate of *Z* may be unreliable. This might have resulted in too large *Z*-values (Hosking and Wallis, 1997), indicating that at least the generalized extreme value (GEV) distribution with Z=2.03, and therefore also the Gumbel distribution, potentially had acceptable fits as well.

In the literature, it is common that the GEV distribution is used. For example, in a national assessment of the rainfall frequency regime of the United States, the GEV distribution was selected to represent daily AMAX series rainfall data (Bonnin et al., 2006). Also in regional analyses of other parts of Italy, e.g. Tuscany (Crisci et al, 2002) and Northern central Italy (Franchini and Galeati, 1994 and Brath et al., 1998 cited by Di Baldassarre et al., 2006), the GEV distribution has been shown to be a suitable regional distribution for the daily precipitation extremes. In part, this prevalence might be explained by the set of candidate distributions used; not every study adopts the attitude of Hosking and Wallis (1997) that other distributions than extreme value distributions should be considered.

The estimated 100-year storm for site 90462 near Trento is comparable to the severe flood event in 1966, where 140-160 mm of rain fell over 2 days at the location of this site (Malguzzi et al., 2006). The fact that the 134 mm measured at this site on January 31–February 1 in 1986 did not coincide with an increase at the nearby discharge site highlights that it is not only the magnitude of an extreme precipitation event that has an impact on floods, but also the timing.

To perform a flood risk assessment for the Adige basin, the results from the regional frequency analysis of precipitation extremes might be used as input to a rainfall-runoff model to estimate the flood frequency curve. This would likely be a preferable approach even if the region had been found homogenous for discharge, due to the poor data availability. This might require the index storm to be predicted at ungauged sites. The appropriate method might be found using the framework of Bocchiola et al. (2003).

5.5. L-MOMENTS AND MEAN ANNUAL PRECIPITATION

In previous studies where significant relationships between L-moments and MAP has been established (e.g. Schaefer, 1990; Di Baldassarre et al., 2006), MAP is used to define regions. Sites within a short interval of MAP are grouped and regional L-moments are calculated from the models. These relationships can then be used to assign an arbitrary site to a region, given that the MAP is known over the whole area. In effect, this allows the prediction of design storms at ungauged sites.

The applicability of the linear relationships between the selected L-moments and MAP could be more thoroughly examined in Monte Carlo simulations. Many samples would be generated from the regional distribution and used to calculate a confidence interval. The capability of the model to reproduce the rainfall extremes could then be assessed by looking at the percentage of samples falling outside the confidence interval (see Di Baldassarre et al., 2006 for a detailed description).

However, assuming the linear relationships in this study to be true, it would still not be meaningful to subdivide sites into groups according to MAP. At least not for L-CV, where the slope is close to zero, meaning that the regional L-CVs would be more or less the same: for the observed MAP, the range would be 0.165-0.175.

It is also noted that the range of MAP is significantly shorter for the Adige basin than in the study areas of Schaefer (1990) and Di Baldassarre et al. (2006). However, the observed range covers 500-1000 mm which is the interval where the decrease in L-moments is most notable in these studies.

5.6. SEASONALITY ANALYSIS

The mean timing of both precipitation and discharge maxima in the Adige basin are in line with results of larger scale studies using data from similar time periods (Blöschl et al., 2017; Parajka et al., 2010).

Monthly distributions of discharge and precipitation AMAX occurrences had single peaks. This shows that D_{mean} values are not averages of two annual peaks, say snow melt in spring and heavy rainfall in autumn in the case of discharge maxima. The observation that the monthly distribution peak, as well as D_{mean} values, of discharge have earlier timing indicates that precipitation maxima do not necessarily trigger extreme flows, and that other generation processes play an important role. Given the high elevation of the basin and that discharge maxima typically occur in summer, the peak flows are most likely linked to snow melt (Parajka et al., 2010). It has been shown that the main effect of snow melt often is not the direct input of water to streams, but to increase antecedent soil moisture (Parajka et al., 2010), thus amplifying the impact on stream flow of rainfall events. The observed discharge peaks are likely an effect of the interplay between melting snow, rain-on-snow events and heavy precipitation. A more complete picture of the hydrometeorological regimes would be gained by analyzing the seasonality of soil moisture and temperature together with that of precipitation and discharge.

The influence of dam regulation must also be considered. A study by Zolezzi et al. (2009) suggested that seasonal variation of discharge in Adige lessened because of the reservoirs built before the 1960s and still in use today. However, there is not a notable observed difference in either D_{mean} or r for sites in streams unaffected by reservoirs and for those downstream a reservoir. This indicates that the observed seasonality is governed by natural processes.

Dam regulation might however explain the lower variability of discharge β-values, as the regulation may dampen variations in timing. The shift in discharge maxima was small, and it was difficult to assess potential causes without analyzing the temporal evolution of floods together with that of flood generation processes. While it was quite unexpected to see a shift to later floods, considering that climate change might rather cause earlier snow melts, the result for discharge shifts corresponded to that of Blöschl et al. (2017).

5.7. UNCERTAINTIES

This section aims at addressing uncertainties that has not been covered in the above sections.

5.7.1. Data

It should be noted that time series in the database used in this study might be influenced by measurement errors. Information about type and placement of gauges, correction methods used etc. has not been available. Discharge data is often converted from measured water levels via rating curves; for flood data, the errors associated with estimated curves might be high. Typical precipitation errors include influence of wind, wetting and evaporation losses, blowing snow etc. These types of errors should be exacerbated for observations of extreme values. It has been assumed that corrections for such errors have been made for the data labelled with verified quality. Unverified data has been included in the study, and potential errors are likely associated with an underestimation of the true values, and results should be on the conservative side. This does of course not account for reporting errors, calibration errors etc., which are an unknown source of uncertainty.

The poor availability of discharge data and the presence of reservoirs in the stream network have made the interpretation of the discharge statistics difficult, at least in analyses of trends and L-moments. When comparing the results of the seasonality analysis to previous studies mentioned in the above section, the availability of discharge data seems to have been adequate.

5.7.2. Serial correlation

The AMAX series were found to be affected by serial correlation to a degree. In the trend analysis, this was addressed by incorporating the method of Yue et al. (2002) which should minimize the influence on those results. For the regional frequency analysis of precipitation however, no steps were taken to reduce serial dependence. Landwehr et al. (1979) studied the effect of serial correlation on estimation of parameters and quantiles of the Gumbel distribution with probability weighted moments. They found that the efficiency of the estimates decreased when using data randomly generated from a process with a serial correlation coefficient of 0.5 (higher than the maximum coefficient observed in this study). Hosking and Wallis (1997) concluded from the results of Landwehr et al. (1979) that a small amount of serial dependence does not greatly affect the quality of quantile estimates. Schaefer (1990) found an average serial correlation of the magnitude 0.027 and considered that to be negligible (although no variance or range of coefficients was reported). The average serial correlation found in this study was 0.024 for precipitation.

The approach has been to use the data as it is, but there could be an argument for excluding series with a serial correlation coefficient above a certain threshold. It could also be possible to reduce serial dependence of series by shifting the hydrological years to minimize the risk of maxima being generated from the same meteorological phenomena.

5.7.3. Selection procedure

The procedure for selecting appropriate time series aimed at being thorough, but one could argue it to subjective. To mitigate this, a validation of the method such as in Papalexiou and Koutsoyiannis (2013) could be used. There, a Monte Carlo scheme was set up to find appropriate threshold values for the criteria by selecting a complete subset of

the record, finding the annual maxima and then modifying it to contain missing values. Annual maxima were then extracted from the modified subset by the proposed method with various criteria values. Finally, the two sets of annual maxima were compared to conclude which criteria values gave the best result.

5.8. A NOTE ON SCALES

In this study, precipitation and discharge extremes in the relatively small Adige river basin have been investigated to find their spatial and temporal characteristics, using daily data. However, if for example hourly precipitation had been analyzed instead, it may have shown to be much more influenced by convective summer storms and thus have a more well-defined seasonality, but also a larger degree of heterogeneity in L-moments. So, it is important to remember that the patterns that have emerged here ultimately depend on the chosen scale, both of time and space.

6. CONCLUSIONS

In this study, the characteristics of daily precipitation and discharge extremes in the Adige river basin down to the city of Trento were described. Annual maximum series for the period 1975–2014 were analyzed in terms of trends, seasonality and L-moments. The research questions may be answered as follows.

1. A weak but significant signal of decreasing extremes was detected in the study period. A minority of the AMAX series of precipitation and discharge showed predominantly negative trends. The percentages of sites with significant negative trends were overall larger than the significance levels, i.e. more than is expected to be explained by randomness.
2. (a) The Adige basin was found to be homogenous with respect to precipitation. The results do not support the assumption that the basin can be considered as a homogenous region for discharge. (b) The Pearson type III and generalized normal distributions were both found to be adequate regional frequency distributions for precipitation maxima. (c) The estimated annual maximum daily precipitation at Trento was between 114 and 148 mm/d for a 100-year return period.
3. (a) A possible explanation for the spatial distribution of sample precipitation L-moments was the main storm direction during autumn. (b) A weak relationship between mean annual precipitation (MAP) and both L-CV and L-skewness was observed, where the L-moment ratios showed a tendency to decrease with increasing MAP. A linear model was significant at the 10% level for L-skewness.
4. (a) Precipitation extremes were characterized primarily by autumn storms, although the seasonality was rather weak. Discharge had a stronger seasonality with peaks occurring mainly in June and July. (b) This meant that the timing was not solely explained by rainfall maxima. (c) A minor shift towards later floods was observed.

Further research on the Adige basin could focus on the findings of the trend analysis. If only precipitation data is used, it would be possible to extend the time period and test if the negative trends prevail. Another focus could be the application and calibration of a rainfall-runoff model to predict floods in the basin, using the index storm developed here as input.

7. REFERENCES

Adamkowski, K. 2000. Regional analysis of annual maximum and partial duration flood data by nonparametric and L-moment methods. *Journal of Hydrology*. [e-journal] 229(2000), 219–231. doi: 10.1016/S0022-1694(00)00156-6.

Alexander, L.V., Zhang, X., Peterson, T.C., Caesar, J., Gleason, B., Klein Tank, A.M.G., Haylock, M., Collins, D., Trewin, B., Rahimzadeh, F., Tagipour, A., Rupa Kumar, K., Revadekar, J., Griffiths, G., Vincent, L., Stephensson, D.B., Burn, J., E. Aguilar, E., Brunet, M., Taylor, M., New, M., Zhai, P., Rusticucci, M., Vazquez-Aguirre, J.L. 2006. Global observed changes in daily climate extremes of temperature and precipitation. *Journal of Geophysical research*. [e-journal] 11. doi:10.1029/2005JD006290.

Alkema, D., Zanchi, A., De Amicis, M. 2003. Geomorphologic Map of the Adige valley, north of Trento, Italy. *Studi Trentini di Scienze Naturali – Acta Geologica*. 78(2001), 147-153.

Allamano, P., Claps, P., Laio, F. 2009. Global warming increases flood risk in mountainous areas. *Geophysical Research Letters*, [e-journal] 36(24). doi:10.1029/2009GL041395

Bayliss, A.C., Jones, R.C. 1993. *Peaks-over-threshold flood database: Summary statistics and seasonality*.Wallingford: Institute of Hydrology.

Blöschl, G., Sivapalan, M., Wagener, T., Viglione, A. and Savenije, H. (eds). 2013. *Runoff Prediction in Ungauged Basins: Synthesis across Processes, Places and Scales*. [e-book] Cambridge: Cambridge University Press. doi: 10.1017/CBO9781139235761.

Blöschl, G., Hall, J., Parajka, J., Perdigão, R.A.P., Merz, B., Arheimer, B., Aronica, G.T., Bilibashi, A., Bonacci, O., Borga, M., Čanjevac, I., Castellarin, A., Chirico, GB., Claps, P., Fiala, K., Frolova, N., Gorbachova, L., Gül, A., Hannaford, J., Harrigan, S., Kireeva, M., Kiss, A., Kjeldsen, T.R., Kohnová, S., Koskela, J.J., Ledvinka, O., Macdonald, N., Mavrova-Guirguinova, M., Mediero, L., Merz, R., Molnar, P., Montanari, A., Murphy, C., Osuch, M., Ovcharuk, V., Radevski, I., Rogger, M., Salinas, J.L., Sauquet, E., Šraj, M., Szolgay, J., Viglione, A., Volpi, E., Wilson, D., Zaimi, K., Živković, N. 2017. Changing climate shifts timing of European floods. *Science*. [e-journal] 357(6351), 588-590. doi: 10.1126/science.aan2506.

Bocchiola, D., De Michele, C., Rosso, C. 2003. Review of recent advances in index flood estimation. *Hydrology and Earth System Sciences*. [e-journal] 7(3), 283-296. doi: 10.5194/hess-7-283-2003.

Bonnin, G.M., Martin, D., Lin, B., Parzyok, T., Yekta, M.and Riley, D. 2006. *Precipitation-Frequency Atlas of the United States, Volume 1, Version 4.0: Semiarid Southwest (Arizona, Southeast California, Nevada, New Mexico)*. NOAA Atlas 14

Castellarin, A., Burn, D.H., Brath, A. 2008. Homogeneity testing: How homogeneous do heterogeneous cross-correlated regions seem? *Journal of Hydrology*. [e-journal] 360, 67– 76. doi:10.1016/j.jhydrol.2008.07.014.

Crisci, A., Gozzini, B., Meneguzzo, F., Pagliara, S., Maracchi, G. 2002. Extreme rainfall in a changing climate: regional analysis and hydrological implications in Tuscan. *Hydrol. Process*. 16, 1261–1274.

COST, 2012. *Review of applied-statistical methods for flood-frequency analysis in Europe*. Centre for Ecology & Hydrology.

Dalrymple, T. 1960. *Flood-frequency analyses, Manual of Hydrology: Part 3*. [pdf] U.S. G.P.O. Available at: < https://pubs.er.usgs.gov/publication/wsp1543A > [Accessed 6 February 2018].

Di Baldassarre, G., Castellarin, A., Brath, A. 2006. Relationships between statistics of rainfall extremes and mean annual precipitation: an application for design-storm estimation in northern central Italy. *Hydrol. Earth Syst. Sci.* [e-journal] 10, 589–601. doi: 10.5194/hess-10-589-2006.

Dowle, M., Srinivasan, A., Gorecki, J., Short, T., Lianoglou, S., Antonyan, E. 2017. *data.table: Extension of 'data.frame'.* https://CRAN.R-project.org/package=data.table.

Eaton, B., Church, M., Ham, D. 2002. Scaling and regionalization of flood flows in British Columbia, Canada. *Hydrol. Process*. [e-journal] 16, 3245–3263. doi: 10.1002/hyp.1100.

Encyclopædia Britannica, 1998. *Adige River*. [online] Available at: < https://www.britannica.com/place/Adige-River> [Accessed: 6 February 2018]

Ferreira, A., De Haan, L. 2015. On the block maxima method in extreme value theory: PWM estimators. *The Annals of Statistics*. [e-journal] 43(1), 276-298. doi:10.1214/14-AOS1280

Hailegeorgis, T.T., Thorolfsson, S.T., Alfredsen, K. 2013. Regional frequency analysis of extreme precipitation with consideration of uncertainties to update IDF curves for the city of Trondheim. *Journal of Hydrology*. [e-journal] 498(2013), 305–318. doi: 10.1016/j.jhydrol.2013.06.019

Hall, J., Blöschl, G., 2017. Spatial Patterns and Characteristics of Flood Seasonality in Europe. *Hydrol. Earth Syst. Sci. Discuss.* [e-journal] https://doi.org/10.5194/hess-2017-649

Helsel, D.R. and R. M. Hirsch, 2002. *Statistical Methods in Water Resources Techniques of Water Resources Investigations*, Book 4, chapter A3. U.S. Geological Survey. 522 pages.

Hosking, J.R.M. 2015. *lmom: L-Moments*. https://CRAN.R-project.org/package=lmom.

Hosking, J.R.M. 2017. *lmomRFA: Regional Frequency Analysis using L-Moments*. https://CRAN.R-project.org/package=lmomRFA.

Hosking, J.R.M. and Wallis, J.R. 1997. *Regional frequency Analysis.* New York: Cambridge University Press.

Katz, R.W., Parlange, M.B., Naveau, P. 2002. Statistics of extremes in hydrology. *Advances in Water Resources*. 25, 1287–1304.

Klemeš, V. 2000. Tall Tales about Tails of Hydrological Distributions I. *Journal of Hydrologic Engineering*. [e-journal] 5(3). doi: 10.1061/(ASCE)1084-0699(2000)5:3(227).

Landwehr, J. M., Matalas, N. C, and Wallis, J. R. 1979. Probability-weighted moments compared with some traditional techniques in estimating Gumbel parameters and quantiles. *Water Resources Research*, 15, 1055-64.

Malguzzi, P., Grossi, G., Buzzi, A., Ranzi, R., Buizza, R. 2006. The 1966 ‘‘century’’ flood in Italy: A meteorological and hydrological revisitation. *Journal of Geophysical Research*, Vol. 111(D24106). doi:10.1029/2006JD007111

Manfreda, S., Fiorentino, M. 2008. Flood Volume Estimation and Flood Mitigation: Adige River Basin. In: Wiegandt, E. (ed). 2008. *Mountains: Sources of Water, Sources of Knowledge*. Dordrecht: Springer. Ch.15.

Mann, H.B. 1945. Nonparametric Tests Against Trend. *Econometrica*. [e-journal] 13(3), 245-259. doi: 10.2307/1907187.

Mardia, K.V. 1975. *Statistics of Directional Data*. [online]. Available at: < http://www.jstor.org/stable/2984782> [Accessed 6 October 2017].

Merz, R., Blöschl, G. 2003. A process typology of regional floods. *Water Resources Research*. [e-journal] 39(12). doi:10.1029/2002WR001952.

Papalexiou, S.M. and Koutsoyiannis, D. 2013. Battle of extreme value distributions: A global survey on extreme daily rainfall. *Water Resour. Res*. [e-journal] 49, doi:10.1029/2012WR012557

Parajka, J., Merz, R., Blöschl, G. 2005. A comparison of regionalization methods for catchment model parameters. *Hydrology and Earth System Sciences*, [e-journal] 9, 157-171. doi: 10.5194/hess-9-157-2005.

Parajka, J., Kohnová, S., Bálint, G., Barbuc, M., Borga, M., Claps, P., Cheval, S. Dumitrescu, A., Gaume, E., Hlavčová, K., Merz, R., Pfaundler, M., Stancalie, G., Szolgay, J., Blöschl, G. Seasonal characteristics of flood regimes across the Alpine–Carpathian range. *Journal of Hydrology*, [e-journal] 394(1–2), 78-89.doi: 10.1016/j.jhydrol.2010.05.015.

Patakamuri, S.K. 2017. *modifiedmk: Modified Mann Kendall Trend Tests*. https://CRAN.R-project.org/package=modifiedmk.

Persiano, S., Castellarin, A., Salinas, J.L., Domenghetti, A., Brath, A. Climate, orography and scale controls on flood frequency in Triveneto (Italy). *Proc. IAHS*, [e-journal] 373, 95–100. doi: 10.5194/piahs-373-95-2016.

Schaefer, M.G., Regional analyses of precipitation annual maxima in Washington State. Water Resources Research. [e-journal] 26(1). doi: 10.1029/WR026i001p00119.

Sen, P.K. 1968. Estimates of the Regression Coefficient Based on Kendall's Tau. *Journal of the American Statistical Association*. [e-journal] 63(324), 1379-1389. doi: 10.2307/2285891.

Siler, N. and Roe, G. 2014. How will orographic precipitation respond to surface warming? An idealized thermodynamic perspective. *Geophys. Res. Lett.* [e-journal] 41, 2606–2613, doi:10.1002/2013GL059095.

Theil, H. 1950. A rank-invariant method of linear and polynomial regression analysis. I, II, III. *Nederl. Akad. Wetensch., Proc*. 53, 386–392, 521–525, 1397–1412.

U.S. Geological Survey, 2015. *Global Multi-resolution Terrain Elevation Data 2010 (GMTED2010*). [online] Available at: < https://lta.cr.usgs.gov/GMTED2010> [Accessed: 6 February 2018]

Viglione, A., Chirico, G.B., Komma, J., Woods, R., Borga, M., Blöschl, G. 2010. Quantifying space-time dynamics of flood event types. *Journal of Hydrology*. [e-journal] 394, 213–229. doi:10.1016/j.jhydrol.2010.05.041.

Westfall, P.H. 2014. Kurtosis as Peakedness, 1905 – 2014. R.I.P. *The American statistician*. 68(3):191-195. doi:10.1080/00031305.2014.917055.

Westra, S., Alexander, L.V., Zwiers, F.W. 2012. Global Increasing Trends in Annual Maximum Daily Precipitation. [e-journal] *Journal of Climate*. 26. doi:10.1175/JCLI-D-12-00502.1.

Yue, S., Pilon, P., Phinney, B., Cavadias, G. The influence of autocorrelation on the ability to detect trend in hydrological series. *Hydrological Processes*. [e-journal] 16, 1807-1829. doi:10.1002/hyp.1095.

Zolezzi, G., Bellin, A., Bruno, M.C., Maiolini, B., Siviglia, A. 2009. Assessing hydrological alterations at multiple temporal scales: Adige River, Italy. *Water Resources Research*. 45. doi:10.1029/2008WR007266.

APPENDIX

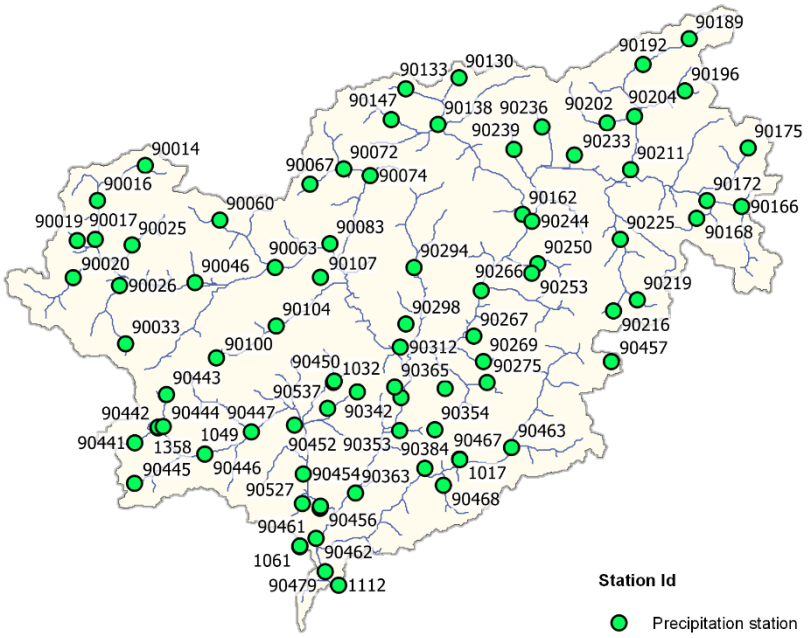

Figure A1. Locations of selected precipitation sites. Labels are site IDs

Table A1. Summary of results for each precipitation site grouped by L-moments, discordancy measure (*D*), seaonality indices (D_{mean} and *r*) and trend analysis (Kendall's τ and p-value)

Site ID	Record length	L-location	L-CV	L-skewness	L-kurtosis	D	Dmean	r	τ	p
1017	27	54.5	0.19	0.26	0.30	-	256	0.46	-0.25	0.08
1032	29	54.0	0.16	0.35	0.27	2.5	267	0.43	-0.16	0.24
1049	31	62.4	0.17	0.17	0.13	0.0	294	0.42	-0.07	0.62
1050	30	68.0	0.18	0.21	0.10	0.4	267	0.36	-0.17	0.20
1061	22	67.5	0.20	0.15	0.00	2.5	258	0.63	-0.09	0.61
1112	30	69.7	0.17	0.24	0.18	0.2	292	0.48	-0.27	0.04
1358	25	56.5	0.15	0.13	0.09	0.3	313	0.09	-0.15	0.31
90014	23	39.2	0.13	-0.06	-0.02	2.8	242	0.35	-0.24	0.13
90016	39	42.1	0.17	0.28	0.14	1.0	228	0.40	-0.11	0.33
90017	39	46.9	0.14	0.23	0.19	1.2	250	0.51	-0.04	0.71
90019	32	48.1	0.14	0.04	0.14	1.4	257	0.37	0.05	0.71
90020	39	44.7	0.16	0.24	0.24	0.8	238	0.15	-0.04	0.72
90025	37	40.5	0.18	0.21	0.15	-	231	0.47	-0.23	0.05
90026	25	39.4	0.16	0.12	0.24	2.0	292	0.46	-0.24	0.11
90033	23	46.5	0.14	0.01	0.19	-	230	0.60	-0.21	0.18
90046	39	43.9	0.18	0.23	0.18	0.3	267	0.42	-0.07	0.55
90060	37	47.7	0.20	0.25	0.17	0.7	273	0.22	0.00	0.99
90063	36	47.0	0.19	0.13	0.00	2.2	253	0.32	-0.03	0.80

Site ID	Record length	L-location	L-CV	L-skewness	L-kurtosis	D	Dmean	r	τ	p
90067	25	67.2	0.18	0.25	0.19	0.3	250	0.36	0.09	0.57
90072	39	90.1	0.19	0.18	0.14	0.3	239	0.51	0.12	0.29
90074	39	65.6	0.18	0.23	0.15	0.2	240	0.48	0.10	0.39
90083	32	54.8	0.19	0.17	0.14	0.4	257	0.28	0.08	0.54
90100	39	68.6	0.18	0.28	0.24	0.8	289	0.48	-0.08	0.47
90104	37	79.8	0.24	0.23	0.16	4.5	266	0.32	-0.03	0.84
90107	38	64.5	0.17	0.10	0.17	1.1	267	0.32	-0.13	0.27
90130	32	52.9	0.20	0.12	0.11	1.5	212	0.51	0.16	0.21
90133	39	60.1	0.15	0.05	0.12	1.0	252	0.45	0.09	0.45
90138	39	49.3	0.18	0.21	0.08	0.6	236	0.54	-0.05	0.67
90147	39	62.3	0.14	0.06	0.05	0.9	219	0.55	-0.05	0.65
90162	39	43.7	0.17	0.22	0.09	0.5	214	0.72	0.05	0.67
90166	39	45.1	0.16	0.11	0.10	0.2	257	0.51	-0.01	0.92
90168	35	55.2	0.19	0.14	0.00	1.9	262	0.58	0.03	0.79
90172	34	46.9	0.15	0.05	0.08	-	244	0.39	0.26	0.03
90175	39	46.8	0.14	0.12	0.13	0.6	226	0.39	0.15	0.19
90189	33	45.8	0.14	0.26	0.21	1.5	239	0.32	-0.02	0.88
90192	29	50.3	0.13	0.15	0.09	1.5	211	0.54	-0.02	0.89
90196	32	48.5	0.18	0.23	0.15	0.2	212	0.38	0.06	0.63
90202	33	55.4	0.14	0.17	0.09	1.0	227	0.65	0.05	0.69
90204	29	49.6	0.17	0.19	0.19	0.2	211	0.60	0.15	0.28
90211	27	48.9	0.17	0.10	0.00	1.3	240	0.54	0.18	0.20
90216	25	60.4	0.14	0.07	0.17	1.4	236	0.47	-0.17	0.26
90219	36	48.8	0.16	0.08	0.07	0.5	273	0.44	-0.05	0.67
90225	33	44.5	0.17	0.24	0.14	0.5	247	0.60	-0.17	0.17
90233	32	44.5	0.18	0.14	0.07	-	222	0.65	0.27	0.03
90236	39	55.4	0.15	0.11	0.14	0.4	256	0.38	0.10	0.37
90239	24	45.5	0.15	0.14	0.21	1.0	218	0.48	0.18	0.25
90244	37	43.0	0.17	0.25	0.13	0.6	215	0.71	-0.03	0.80
90250	35	45.5	0.14	0.13	0.12	-	225	0.62	-0.16	0.20
90253	32	51.7	0.14	0.17	0.07	-	228	0.64	-0.23	0.08
90266	36	45.6	0.17	0.25	0.14	0.5	226	0.57	-0.15	0.21
90267	37	47.3	0.13	0.11	0.05	1.5	213	0.71	-0.03	0.84
90269	34	49.3	0.21	0.37	0.33	-	227	0.45	-0.36	0.00
90275	30	51.3	0.14	0.09	0.13	0.7	234	0.42	-0.08	0.54
90294	39	55.4	0.17	0.08	0.03	0.9	225	0.42	-0.08	0.51
90298	36	54.1	0.17	0.15	0.16	-	238	0.46	-0.19	0.12
90312	39	51.6	0.20	0.28	0.20	0.9	236	0.43	-0.14	0.21
90337	23	47.5	0.18	0.21	0.15	0.2	240	0.63	-0.13	0.43
90342	39	53.3	0.17	0.28	0.12	-	239	0.45	-0.30	0.01
90353	30	56.4	0.15	0.23	0.14	0.6	241	0.44	-0.04	0.78
90354	39	50.8	0.13	0.11	0.07	1.1	230	0.39	-0.06	0.62
90363	29	60.5	0.15	0.12	0.12	0.2	263	0.35	-0.08	0.54
90365	32	53.2	0.16	0.25	0.17	0.4	217	0.39	-0.11	0.38
90384	37	57.0	0.16	0.12	0.07	-	252	0.40	-0.21	0.08

Site ID	Record length	L-location	L-CV	L-skewness	L-kurtosis	D	Dmean	r	τ	p
90441	21	62.0	0.14	-0.04	0.09	2.6	303	0.35	-0.13	0.46
90442	31	54.7	0.16	0.09	0.12	0.4	296	0.20	-0.25	0.05
90443	27	46.8	0.14	0.15	0.17	0.8	235	0.37	-0.09	0.54
90444	34	51.6	0.15	0.24	0.14	0.9	310	0.21	-0.03	0.79
90445	25	72.4	0.14	0.10	0.13	0.7	258	0.39	-0.19	0.21
90446	33	61.8	0.16	0.19	0.15	0.1	297	0.45	-0.09	0.49
90447	31	59.3	0.18	0.20	0.15	0.2	295	0.22	-0.19	0.15
90450	29	54.0	0.16	0.35	0.27	2.5	267	0.43	-0.16	0.24
90451	29	63.7	0.18	0.32	0.21	1.0	282	0.53	-0.20	0.14
90452	31	62.2	0.18	0.14	0.19	1.0	287	0.33	-0.13	0.32
90454	23	76.5	0.15	0.12	0.01	1.2	295	0.46	0.02	0.91
90456	31	67.5	0.18	0.20	0.13	0.1	272	0.37	-0.19	0.14
90457	25	74.5	0.18	0.08	0.15	1.5	258	0.58	-0.04	0.78
90461	25	66.8	0.19	0.18	0.05	1.2	262	0.67	-0.12	0.44
90462	22	66.7	0.18	0.13	0.02	1.2	306	0.33	-0.10	0.53
90463	24	68.0	0.19	0.25	0.23	0.8	291	0.27	0.06	0.71
90467	27	54.5	0.19	0.26	0.30	-	256	0.46	-0.25	0.08
90468	29	66.9	0.18	0.17	0.08	0.3	281	0.49	0.00	0.98
90479	33	68.7	0.16	0.22	0.16	-	291	0.59	-0.33	0.01
90527	32	71.9	0.19	0.12	0.14	1.4	269	0.40	-0.17	0.17
90537	36	62.1	0.19	0.28	0.24	-	273	0.50	-0.20	0.09

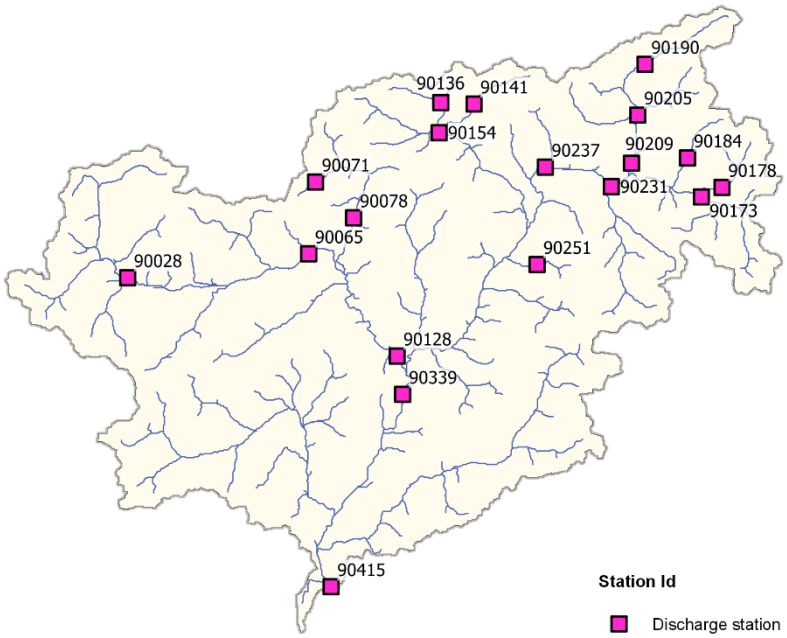

Figure A2. Locations of selected discharge sites. Labels are site IDs

Table A2. Summary of results for each discharge site grouped by L-moments, discordancy measure (*D*), seaonality indices (D_{mean} and *r*) and trend analysis (Kendall's τ and p-value)

Site ID	Record length	L-location	L-CV	L-skewness	L-kurtosis	D	md	r	τ	p
90028	28	3.2	0.18	0.20	0.19	0.5	187	0.69	0.08	0.59
90065	33	5.1	0.18	0.21	0.16	0.1	205	0.81	-0.02	0.88
90128	37	7.0	0.23	0.25	0.13	0.5	209	0.65	-0.22	0.06
90136	23	25.3	0.24	0.41	0.25	2.9	201	0.55	-0.31	0.05
90141	23	15.6	0.14	0.33	0.26	1.7	185	0.85	-0.11	0.50
90154	39	18.9	0.23	0.29	0.18	0.8	212	0.61	-0.10	0.37
90173	33	4.5	0.18	0.24	0.12	0.5	196	0.54	0.02	0.88
90178	30	6.4	0.15	0.26	0.16	0.5	178	0.73	-0.24	0.07
90184	26	9.0	0.19	0.08	0.14	2.0	185	0.85	-0.06	0.69
90190	29	18.7	0.13	0.15	0.18	1.0	181	0.91	-0.01	0.95
90205	31	14.5	0.14	0.12	0.18	1.3	184	0.92	0.07	0.62
90209	27	14.3	0.16	0.34	0.24	0.9	183	0.92	-0.19	0.17
90231	32	7.5	0.21	0.27	0.13	0.4	212	0.51	0.05	0.73
90237	37	7.3	0.15	0.28	0.17	1.0	189	0.77	-0.11	0.36
90251	20	8.9	0.20	0.29	0.11	0.9	220	0.41	-0.19	0.26
90339	39	7.1	0.18	0.19	0.08	-	193	0.68	-0.31	0.01
90415	33	7.1	0.23	0.21	0.08	1.1	215	0.54	-0.33	0.01

Table A3. Results of sensitivity analysis of precipitation trends, with p-values averaged for each site and for each percentage of artificial gaps. Results are shown only for sites with p-values < 0.10 (10% significance).

Artificial gaps	Site ID	Avg. p-value
0%	1112	0.045
	90025	0.055
	90233	0.032
	90253	0.077
	90342	0.008
5%	1112	0.071
	90025	0.067
	90233	0.035
	90342	0.016
10%	1112	0.087
	90025	0.088
	90233	0.038
	90342	0.027
15%	90233	0.044
	90342	0.037
20%	90233	0.048
	90342	0.050
25%	90233	0.057
	90342	0.064

Table A4. Results of sensitivity analysis of discharge trends, with p-values averaged for each site and for each percentage of artificial gaps. Results are shown only for sites with p-values < 0.10 (10% significance).

Artificial gaps	Site ID	Avg. p-value
0%	90136	0.048
	90178	0.069
	90339	0.006
5%	90136	0.064
	90339	0.017
10%	90136	0.082
	90339	0.033
15%	90339	0.052
20%	90339	0.077
25%	-	-

In this section, formulas of the probability density functions $f(x)$, cumulative distribution functions $F(x)$ and quantile functions $x(F)$ are given (when defined) for the probability distributions included in this study. These expressions follow the parametrization of Hosking and Wallis (1997) and Hosking (2015).

Gumbel distribution

Parameters: ξ (location) and α (scale).

$$f(x) = \alpha^{-1} \exp\{-(x-\xi)/\alpha\} \exp[-\exp\{-(x-\xi)/\alpha\}] \quad \text{(A1)}$$

$$F(x) = \exp[-\exp\{-(x-\xi)/\alpha\}] \quad \text{(A2)}$$

$$x(F) = \xi - \alpha \log(-\log F) \quad \text{(A3)}$$

Generalized Pareto distribution

Parameters: ξ (location), α (scale) and k (shape).

$$f(x) = \alpha^{-1} e^{-(1-k)y}, \qquad y = \begin{cases} -k^{-1} log\{1-k(x-\xi)/\alpha\}, & k \neq 0 \\ (x-\xi)/\alpha\,, & k = 0 \end{cases} \quad \text{(A4)}$$

$$F(x) = 1 - e^{y} \quad \text{(A5)}$$

$$x(F) = \begin{cases} \xi + \alpha\{1-(1-F)^k\}/k, & k \neq 0 \\ \xi - \alpha \log(1-F)\,, & k = 0 \end{cases} \quad \text{(A6)}$$

Generalized normal distribution

Parameters: ξ (location), α (scale) and k (shape).

$$F(x) = \Phi(y), \qquad y = -(1/k)\log\{1-k(x-\xi)/\alpha\} \quad \text{(A7)}$$

$x(F)$ has no explicit analytical form. $k < 0$ is the three-parameter lognormal distribution, $k = 0$ is the normal distribution, and $k > 0$ is the reverse lognormal distribution.

Generalized extreme-value distribution

Parameters: ξ (location), α (scale) and k (shape).

$$f(x) = \alpha^{-1} e^{-(1-k)y - e^{-y}}, \quad y = \begin{cases} -k^{-1} log\{1-k(x-\xi)/\alpha\}, & k \neq 0 \\ (x-\xi)/\alpha\,, & k = 0 \end{cases} \quad \text{(A8)}$$

$$F(x) = e^{-e^{-y}} \quad \text{(A9)}$$

$$x(F) = \begin{cases} \xi + \alpha\{1-(\log F)^k\}/k, & k \neq 0 \\ \xi - \alpha \log(-\log F)\,, & k = 0 \end{cases} \quad \text{(A10)}$$

Three types of extreme-value distributions with cumulative distribution functions as follows:

Type I: $F(x) = \exp(e^{-x}), \quad -\infty \le x \le \infty$ (A11)

Type II: $F(x) = \exp\left(-x^{-\delta}\right), \quad 0 \le x \le \infty$ (A12)

Type III: $F(x) = \exp(-|x|^{\delta}), \quad -\infty \le x \le 0$ (A13)

Corresponding to $k = 0$, $k < 0$ and $k > 0$.

Generalized logistic distribution

Parameters: ξ (location), α (scale) and k (shape).

$$f(x) = \frac{\alpha^{-1}e^{-(1-k)y}}{(1+e^{-y})^2}, \quad y = \begin{cases} -k^{-1}log\{1-k(x-\xi)/\alpha\}, & k \neq 0 \\ (x-\xi)/\alpha\,, & k = 0 \end{cases} \quad \text{(A14)}$$

$$F(x) = 1/(1+e^{-y}) \quad \text{(A15)}$$

$$x(F) = \begin{cases} \xi + \alpha[1-\{(1-F)/F\}^k]/k, & k \neq 0 \\ \xi - \alpha\log\{(1-F)/F\}, & k = 0 \end{cases} \quad \text{(A16)}$$

Pearson type III distribution

Parameters: μ (location), σ (scale) and γ (shape).

When $\gamma \neq 0$, let

$$\alpha = 4/\gamma^2, \quad \text{(A17)}$$

$$\beta = 0.5\,\sigma|\gamma| \quad \text{(A18)}$$

and

$$\xi = \mu - 2\sigma/\gamma. \quad \text{(A19)}$$

For $\gamma > 0$,

$$f(x) = \frac{(x-\xi)^{\alpha-1}e^{-(x-\xi)/\beta}}{\beta^{\alpha}\Gamma(\alpha)} \quad \text{(A20)}$$

$$F(x) = G\left(\alpha, \frac{x-\xi}{\beta}\right)/\Gamma(\alpha) \quad \text{(A21)}$$

where $\Gamma(.)$ is the gamma function,

$$\Gamma(x) = \int_0^{\infty} t^{x-1}e^{-t}dt \quad \text{(A22)}$$

$G(.)$ is the incomplete gamma function,

$$G(\alpha, x) = \int_0^{\infty} t^{\alpha-1}e^{-t}dt \quad \text{(A23)}$$

If $\gamma = 0$, the distribution becomes the Normal distribution. If $\gamma < 0$, then

$$f(x) = \frac{(\xi - x)^{\alpha - 1} e^{-(\xi - x)/\beta}}{\beta^{\alpha} \Gamma(\alpha)} \tag{A24}$$

$$F(x) = 1 - G\left(\alpha, \frac{\xi - x}{\beta}\right) / \Gamma(\alpha) \tag{A25}$$

In each case of γ, $x(F)$ lacks an explicit analytical form.

Kappa distribution

Parameters: ξ (location), α (scale), k and h.

$$f(x) = \alpha^{-1}\{1 - k(x - \xi)/\alpha\}^{1/k - 1}\{F(x)\}^{1 - h} \tag{A26}$$

$$F(x) = \left[1 - h\{1 - k(x - \xi)/\alpha\}^{1/k}\right]^{1/h} \tag{A27}$$

$$x(F) = \xi + \frac{\alpha}{k}\left\{1 - \left(\frac{1 - F^{h}}{h}\right)^{k}\right\} \tag{A28}$$

$h = -1$ is the generalized logistic distribution, $h = 0$ is the generalized extreme-value distribution, and $h = 1$ is the generalized Pareto distribution.